DESIGN AND CONTROL OF A

POWERED TRANSFEMORAL PROSTHESIS

By

Frank Charles Sup IV

Thesis

Submitted to the Faculty of the

Graduate School of Vanderbilt University in

partial fulfillment of the requirements

for the degree of

MASTER OF SCIENCE

in

Mechanical Engineering

December, 2006

Nashville, Tennessee

Approved:

Michael Goldfarb

Eric J. Barth

Nilanjan Sarkar

To my wife

ACKNOWLEDGMENTS

I would first like to thank my advisor Dr. Michael Goldfarb for his guidance and support throughout the duration of my masters. He has inspired me to think creatively and independently and has given me an invaluable toolset in tackling complex open-ended problems. I would also like to express my appreciation and gratitude to the members of my thesis committee Dr. Eric Barth and Dr. Nilanjan Sarkar for their time and support.

Furthermore, I would like to acknowledge my wife, Lara, for her continuous encouragement and support of my academic endeavors. Her confidence and faith in me has allowed me to push my abilities past what I thought was possible. In addition, the encouragement I have received from my entire family has been amazing and I have an enormous appreciation for them.

Lastly, I would like to pay tribute to all the members of the Center for Intelligent Mechatronics for their help and guidance. Post-Docs Kevin Fite and Tom Withrow have been invaluable for their advice and assistance throughout my masters work. In particular, I would like to acknowledge Amit Bohara for his contributions to my work, continual drive to perfection and outstanding advice and critique.

TABLE OF CONTENTS

Page

Appendix

LIST OF FIGURES

Page

LIST OF TABLES

CHAPTER I

INTRODUCTION

1. Introduction

The evolution of the lower limb prosthesis over the recent decades has progressed from purely mechanical systems to systems that include microprocessor control. When evaluating the basic function of standard mechanical knee prosthesis, Figure 1-1, their function is to provide constant mechanical damping in order to extract energy from the system and limit the flextion of the knee joint in the back swing to prevent a collision of the knee joint at full extension. These devices allow for restricted mobility of amputees and provide an abnormal gait pattern.

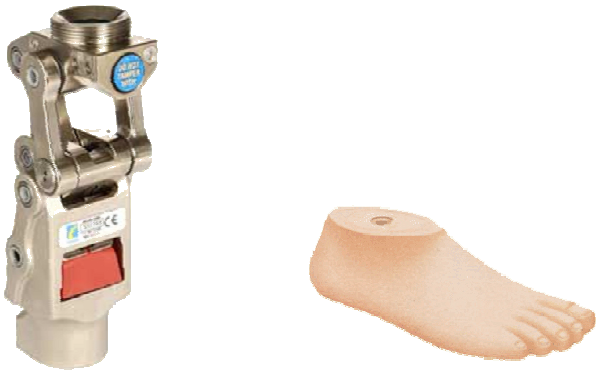

Figure 1-1. Standard lower limb prostheses including mechanical damping knee with locking and solid ankle cushioned heel (SACH) foot.

The current generation of lower limb prosthesis, Figure 1-2, incorporate microprocessors to control either electromagnetic breaks or magnetic rheological fluid for the modulation of the damping in the knee

throughout the gait cycle. The incorporation of spring elements in the ankle, Figure 1-3, provides some power return in the gait cycle, but is incapable of producing power. The devices do provide users with increased mobility; however they still do not replace the power generation capabilities of the missing limb.

Figure 1-2. The Ossur Rheo knee (left) and the Otto Bock C-Leg (right) represent the cutting edge of microprocesser controlled damping prosthetic knees.

Figure 1-3. The Ottobock Trias Foot represents the a typical spring-action ankle.

Despite these significant technological advances in transfemoral prostheses, commercially available prostheses remain limited to energetically passive devices as seen. That is, the joints of the prosthesis can either store or dissipate energy, but cannot provide net power over a gait cycle. The inability to deliver joint power significantly impairs the ability of lower limb prostheses to restore many locomotive functions,

including walking up stairs and slopes, running, and jumping, all of which require significant net positive power at the knee joint, ankle joint, or both (Winter and Sienko 1988, Nadeau et al. 2003, Riener et al. 1999, Prilutsky et al. 1996, DeVita et al. 1996, Nagano et al. 1998, Jacobs et al. 1996). Further, although less obvious, even biomechanically normal walking requires positive power output at the knee joint and significant net positive power output at the ankle joint (Winter, 1991). Transfemoral amputees walking with passive prostheses have been shown to expend up to 60% more metabolic energy relative to healthy subjects during level walking (Waters et al. 1976) and exert as much as three times the affected-side hip power and torque (Winter 1991), presumably due to the absence of powered joints.

A prosthesis with the capacity to deliver power at the knee and ankle joints would presumably address these deficiencies, and would additionally enable the restoration of biomechanically normal locomotion. Such a prosthesis, however, would require 1) power generation capabilities comparable to an actual limb and 2) a control framework for generating required joint torques for locomotion while ensuring stable and coordinated interaction with the user and the environment.

2. Literature Survey

Though the author is not aware of any prior work on the development of a powered knee and ankle prosthesis, prior work does exist on the development of powered knee transfemoral prostheses and powered ankle transtibial prostheses. Regarding the former, Flowers (1973), Donath (1974), Flowers and Mann (1977), Grimes et al. (1977), Grimes (1979), Stein (1983), and Stein and Flowers (1988) developed a tethered electrohydraulic transfemoral prosthesis that consisted of a hydraulically actuated knee joint tethered to a hydraulic power source and off-board electronics and computation, Figure 1-5. They

subsequently developed an “echo control” scheme for gait control, as described by Grimes et al. (1977), in which a modified knee trajectory from the sound leg is played back on the contralateral side. It should be noted that Flowers (1973) prosthesis was specifically designed for an able-bodied subject and could not be used as-is by an amputee. The device was attached to the able-bodied person with their knee in extreme flexion, which made walking with the device difficult due the unnatural configuration of the leg.

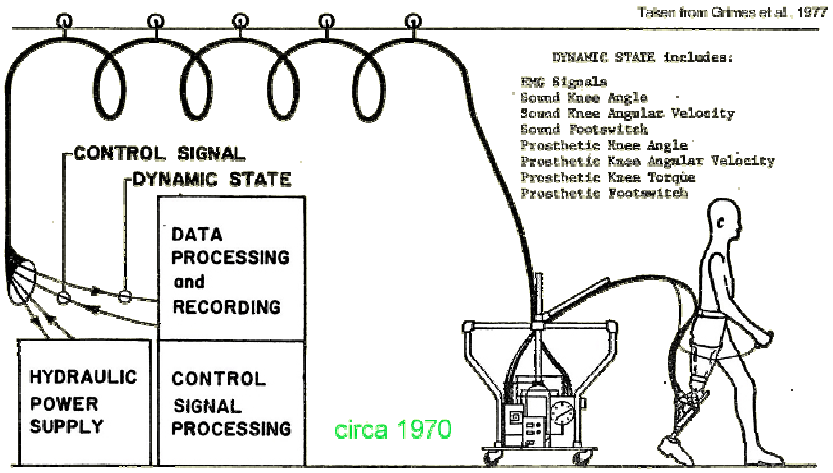

Figure 1-5. Flowers et al. (circa 1970’s) developed a hydraulically actuated knee prosthesis that pioneered the use of active joints.

In addition to this prior work directed by Flowers, other groups have also investigated powered knee joints for transfemoral prostheses. Specifically, Popovic and Schwirtlich (1988) report the development of a battery-powered active knee joint actuated by DC motors, Figure 1-6, together with a finite state knee controller that utilizes a robust position tracking control algorithm for gait control (Popovic et. al., 1995). With regard to powered ankle joints, Klute et al. (1998, 2000) describe the design of an active ankle joint using pneumatic McKibben actuators, although gait control algorithms were not described. Au et al. (2005) assessed the feasibility of an EMG based position control approach for a transtibial prosthesis. Finally,

though no published literature exists, Ossur, a major prosthetics company based in Iceland, has announced the development of both a powered knee and a self-adjusting ankle. The latter, called the “Proprio Foot” (Figure 1-7), is not a true powered ankle, since it does not contribute power to gait, but rather is used to quasistatically adjust the angle of the ankle to better accommodate sitting and slopes. The powered knee, called the “Power Knee” (Figure 1-8), utilizes an echo control approach similar to the one described by Grimes et al. (1977).

Figure 1-6. Electromagnetically actuated powered knee developed by Popovic with the use of a battery pack.

Figure 1-7. Ossur “Proprio” foot used for actively positions the foot for increased functionality.

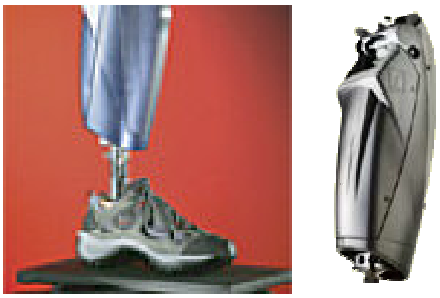

Figure 1-8. Victhom/Ossur “Power Knee” uses electromagnetic actuation and limited battery life.

3. Motivation and Contribution

Unlike any prior work, this thesis describes a prosthesis design that consists of both a powered knee and ankle, and describes a method of control that enables natural, stable interaction between the user and the powered prosthesis. The control approach is implemented on the prosthesis prototype fit to a user, and experimentally shown to provide powered level walking representative of normal gait.

One of the most significant challenges in the development of a powered lower limb prosthesis is providing self-powered actuation capabilities comparable to biological systems. State-of-the-art power supply and actuation technology such as battery/DC motor combinations suffer from low energy density of the power source (i.e., heavy batteries for a given amount of energy), low actuator force/torque density, and low actuator power density (i.e., heavy motor/gearhead packages for a given amount of force or torque and power output), all relative to the human musculoskeletal system. Recent advances in power supply and actuation for self-powered robots, such as the liquid-fueled approaches described by Goldfarb et al. 2003, Shields et al. 2006, Fite et al. 2006, and Fite and Goldfarb 2006, offer the potential of significantly improved energetic characteristics relative to battery/DC motor combinations, and thus bring the potential of a

powered lower limb prosthesis to the near horizon. Specifically, the aforementioned publications describe pneumatic-type actuators, which are powered by the reaction products of a catalytically decomposed liquid monopropellant. The proposed approach has been experimentally shown to provide an energetic figure of merit an order of magnitude greater than state-of-the-art batteries and motors (Shields et al. 2006, Fite and Goldfarb 2006). Rather than construct a self-powered version directly, the authors have developed a power-tethered version of the prosthesis, which enables laboratory-based controller development and prosthesis testing. The self-powered version should be nearly identical to the power-tethered version, but will include an on-board propellant cartridge and catalyst pack in place of the pneumatic tether. This thesis describes the design of the power-tethered pneumatically actuated prosthesis prototype.

4. Organization of the Document

The thesis is organized into five chapters. Chapter I presents the introduction and motivation of the overall powered transfemoral prosthesis concept. The thesis format is to present two manuscripts based on the work and add additional technical detail in the subsequent chapter. Chapter II is a conference paper that has been accepted by the *2006 ASME International Mechanical Engineering Congress and Exposition* as a technical paper. The paper presents the detailed design of a transfemoral prosthesis including the optimization of the kinematic configuration, the overall prosthesis design, model verification with ProE Mechanica Finite Element Analysis (FEA) software, the design of a three-axis socket load cell and the design of an able-bodied adaptor that serves as a laboratory test bed. Chapter III is an addendum to Manuscript I and adds technical details regarding the design, optimization, and socket load cell calibration.

Chapter IV is submitted as a full paper to the *International Journal of Robotics Research* for

consideration in a special issue on “Machines for Human Assistance and Augmentation”. Discussed in this manuscript is the current prosthesis prototype design, methods for converting the prototype to a self-powered version, development of an impedance based control approach and finally presents experimental results for validation of the hardware and control approach. Chapter V is an addendum to Manuscript and adds technical notes regarding the analog electronic circuitry, torque control, and a design summary.

5. References

Au, S. Bonato, P., Herr, H., “An EMG-Postion Controlled System for an Active Ankle-Foot Prothesis: An Initial Experimental Study,” Proceedings of the IEEE Int Conf. on Rehabilitation Robotics, pp. 375-379, 2005.

DeVita, P., Torry M., Glover, K.L., and Speroni, D.L.,“A Functional Knee Brace Alters Joint Torque and Power Patterns during Walking and Running,” Journal of Biomechanics, vol. 29, no. 5, pp. 583-588, 1996.

Donath, M., “Proportional EMG Control for Above-Knee Prosthesis’, Department of Mechanical Engineering Masters Thesis, MIT, 1974.

Fite, K.B., and Goldfarb, M. Design and Energetic Characterization of a Proportional-Injector Monopropellant-Powered Actuator, IEEE/ASME Transactions on Mechatronics, vol. 11, no. 2, pp. 196-204, 2006.

Fite, K.B., Mitchell, J., Barth, E.J., and Goldfarb, M. A Unified Force Controller for a Proportional-Injector Direct-Injection Monopropellant-Powered Actuator, ASME Journal of Dynamic Systems, Measurement and Control, vol. 128, no. 1, pp. 159-164, 2006.

Flowers, W.C., “A Man-Interactive Simulator System for Above-Knee Prosthetics Studies, Department of Mechanical Engineering PhD Thesis, MIT, 1973.

Flowers, W.C., and Mann, R.W., “Electrohydraulic knee-torque controller for a prosthesis simulator,” ASME Journal of Biomechanical Engineering, vol. 99, no. 4, pp. 3-8., 1977.

Goldfarb, M., Barth, E.J., Gogola, M.A. and Wehrmeyer, J.A., “Design and Energetic Characterization of a Liquid-Propellant-Powered Actuator for Self-Powered Robots.,” IEEE/ASME Transactions on

Mechatronics, vol. 8, no. 2, pp. 254-262, 2003.

Grimes, D. L., “An Active Multi-Mode Above Knee Prosthesis Controller. Department of Mechanical Engineering PhD Thesis, MIT., 1979.

Grimes, D. L., Flowers, W. C., and Donath, M., “Feasibility of an active control scheme for above knee prostheses. ASME Journal of Biomechanical Engineering, vol. 99, no. 4, pp. 215-221, 1977.

Jacobs, R., Bobbert, M.F., van Ingen Schenau, G.J.; “Mechanical output from individual muscles during explosive leg extensions: the role of biarticular muscles,” Journal of Biomechanics, vol. 29, no. 4, pp. 513-523, 1996.

Klute, G.K., Czerniecki, J., Hannaford, B., “Development of Powered Prosthetic Lower Limb, Proceedings of the First National Meeting, Veterans Affairs Rehabilitation Research and Development Service, 1998.

Klute, G.K., Czerniecki, J., Hannaford, B., “Muscle-Like Pneumatic Actuators for Below-Knee Prostheses, Proceedings the Seventh International Conference on New Actuators, pp. 289-292, 2000.

Nadeau, S., McFadyen, B.J., and Malouin, F., “Frontal and sagittal plane analyses of the stair climbing task in healthy adults aged over 40 years: What are the challenges compared to level walking?,” Clinical Biomechanics, vol. 18, no. 10, pp. 950-959., 2003.

Nagano, A., Ishige, Y., and Fukashiro, S., “Comparison of new approaches to estimate mechanical output of individual joints in vertical jumps,” Journal of Biomechanics, vol. 31, no. 10, pp. 951-955, 1998.

Popovic, D. and Schwirtlich, L., “Belgrade active A/K prosthesis, “ in de Vries, J. (Ed.), Electrophysiological Kinesiology, Interm. Congress Ser. No. 804, Excerpta Medica, Amsterdam, The Netherlands, pp. 337–343, 1988.

Popovic D, Oguztoreli MN, Stein RB., “Optimal control for an above-knee prosthesis with two degrees of freedom,” Journal of Biomechanics, vol. 28, no. 1, pp. 89-98, 1995.

Prilutsky, B.I., Petrova, L.N., and Raitsin, L.M., “Comparison of mechanical energy expenditure of joint moments and muscle forces during human locomotion,” Journal of Biomechanics, vol. 29, no. 4, pp. 405-415, 1996.

Riener, R., Rabuffetti, M., and Frigo, C., “Joint powers in stair climbing at different slopes.”, Proceedings of the IEEE International Conference on Engineering in Medicine and Biology, vol. 1, p. 530., 1999.

Shields, B.L., Fite, K., and Goldfarb, M. Design, Control, and Energetic Characterization of a Solenoid Injected Monopropellant Powered Actuator, IEEE/ASME Transactions on Mechatronics, vol. 11, no. 4, pp. 477-487, 2006.

Stein, J.L., “Design Issues in the Stance Phase Control of Above-Knee Prostheses,” Department of

Mechanical Engineering PhD Thesis, MIT, 1983.

Stein, J.L., and Flowers, W.C., “Stance phase control of above-knee prostheses: knee control versus SACH foot design,” Journal of Biomechanics, vol. 20, no. 1, pp. 19-28, 1988.

Waters, R., Perry, J., Antonelli, D., and Hislop, H., “Energy cost of walking amputees: the influence of level of amputation,” J. Bone and Joint Surgery. 58A, 42–46, 1976.

Winter, D. A. and Sienko, S. E., “Biomechanics of below-knee amputee gait,” J. Biomechanics. 21, 361–367., 1988.

Winter, D.A., “The biomechanics and motor control of human gait: normal, elderly and pathological,” University of Waterloo Press, 2nd ed., 1991.

CHAPTER II

MANUSCRIPT I: DESIGN OF A PNEUMATICALLY ACTUATED TRANSFEMORAL PROSTHESIS

Frank Sup and Michael Goldfarb

Department of Mechanical Engineering

Vanderbilt University

Nashville, TN 37235

Accepted as a Technical Paper to the

2006 ASME International Mechanical Engineering Congress and Exposition

1. Abstract

This paper describes the design of an above-knee prosthesis with actively powered knee and ankle joints, both of which are actuated via pneumatic actuators. The prosthesis serves as a laboratory test-bed to validate the design and develop of control interfaces for future self-contained versions (i.e., with onboard hot-gas power and computing), and therefore includes a tether for both pneumatic power and control. The prototype prosthesis provides the full range of motion for both the knee and ankle joints while providing 100% of the knee torque required for fast cadence walking and stair climbing and 76% and 100%, respectively, of the ankle torque required for fast cadence walking and for stair climbing, based on the torques required by a healthy 75 kg subject. The device includes sensors to measure knee and ankle torque and position, in addition to a load cell that measures the interaction force and (sagittal and frontal planes) moments between the user and device.

2. Introduction

Despite significant technological advances over the past decade (such as the introduction of microcomputer-modulated damping during swing), commercial transfemoral prostheses remain limited to energetically passive devices. That is, the joints of the prostheses can either store or dissipate energy, but cannot provide any net power over a gait cycle. Today's lower limb transfemoral prosthesis is typically a "locking" knee for stance phase, a passive (sometimes microprocessor modulated) damper at the knee during swing phase, some form of damping at the ankle for heel strike, and often some form of compliant energy storage at the ankle/foot for toe-off. The inability to deliver joint power significantly impairs the ability of these prostheses to restore many locomotive functions, including walking up stairs and slopes,

running, and jumping, all of which require significant net positive power at the knee joint, ankle joint, or both as seen in Fig. 2-1 (Winter and Sienko 1988, Nadeau et al. 2003, Riener et al. 1999, Prilutsky et al. 1996, DeVita et al. 1996, Nagano et al. 1998, Jacobs et al. 1996). Additionally, even during level walking, transfemoral amputees exhibit asymmetric gait kinematics, expend up to 60% more metabolic energy relative to healthy subjects Walters et al. (1976), and exert as much as three times the affected-side hip power and torque relative to healthy subjects Winter (1991), which results in significantly increased socket interface forces. These limitations have a direct impact on the quality of life of many active transfemoral amputees, and most likely speed the onset of degenerative musculoskeletal conditions.

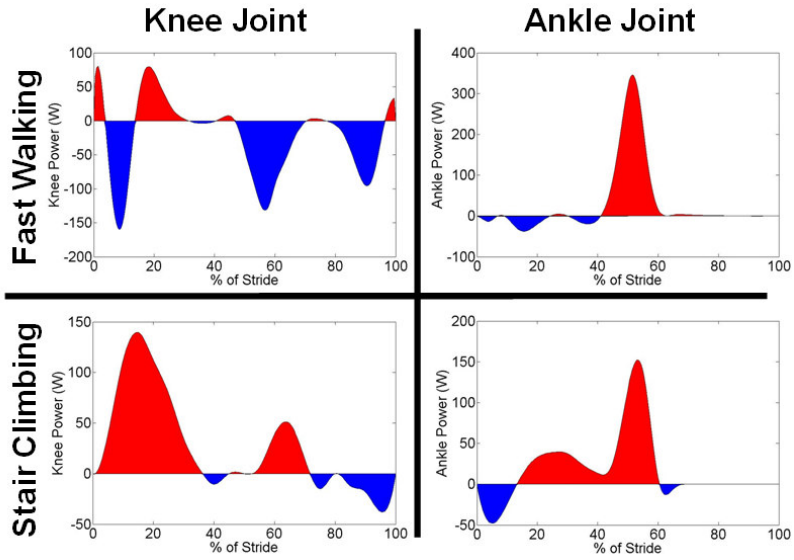

Figure 2-1. Joint power during one cycle for 75 kg normal subjects. Red represents power generated, blue is power dissipated. Winter (1988), Winter and Sienko (1988), Nadeau et al. (2003)

The earliest body of research on actively powered knee joints for transfemoral prostheses was the work by Flowers et al., which took place during the 1970's and 1980's by Flowers (1973), Donath (1974), Grimes et al. (1977), Grimes (1979), Stein (1983), Stein and Flowers (1987). Specifically, Flowers and

Mann (1977) developed a tethered electrohydraulic transfemoral prosthesis that consisted of a hydraulically actuated knee joint tethered to a hydraulic power source and off-board electronics and computation through a tether. The prosthesis did not contain an active ankle joint, but rather incorporated a solid-ankle, cushioned-heel (SACH) foot. The SACH foot effectively absorbed energy at heel strike, although provided relatively little energy storage and return during toe-off. In addition to the body of work directed by Flowers (1973) and Flowers and Mann (1977), other groups have also investigated actively powered knee joints for transfemoral prostheses. Specifically, Popovic and Schwirtlich (1988) report the development of an active knee joint battery-powered DC motor actuated transfemoral prosthesis. Finally, though no published research exists, it should be noted that Ossur, a prosthetics company based in Iceland, has in development an actively powered knee prosthesis for transfemoral amputees. With regard to active ankle joints, Klute et al. (1998, 2000) conducted studies on the use of McKibben actuators in an active ankle joint for transtibial prostheses.

One of the significant challenges in developing a powered lower limb prosthesis is providing on-board power and actuation that is comparable to that of biological systems. Relative to biological systems, state-of-the-art power supply and actuation technology is hindered by the combination of low energy density of the power source (i.e., heavy batteries for a given amount of energy), low actuator force/torque density, and low actuator power density (i.e., heavy motor/gearhead packages for a given amount of force or torque and power output). Recent advances in power supply and actuation for self-powered robots, such as the liquid-fueled approach developed by the investigators Goldfarb et al. (2003), Shields and Goldfarb (2005), Shields et al. (2004) and Fite et al.(2004), offer the potential of significantly improved energetic characteristics, relative to batteries and motors. This paper describes the design of a prototype

transfemoral prosthesis that is intended to be powered by the liquid-fueled approach developed by the investigators. In its initial form, however, the prosthesis will be power-tethered, such that interface and control algorithms can be developed and tested in a laboratory setting. Once such interface and control is developed, the device will be converted for use with on-board power and computation. The remainder of this paper describes the design of the power-tethered prototype.

3. Kinematic Configuration

The kinematic configuration of the actuators was selected via a design optimization to minimize the volume of the actuators, subject to the constraints that they provide the requisite range of motion of the joint and provide a torque/angle phase space that accommodates a 75 kg user during fast walking and stair climbing. The data defining the requisite phase space for fast walking and stair climbing were obtained from Winter (1991) and Nadeau et al. (2003), respectively. Minimum range of motion was determined to be 110° of flexion for the knee and 45° of planterflexion and 20° of dorsiflexion for the ankle.

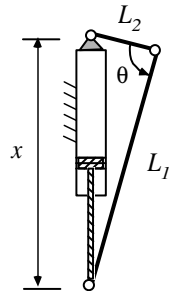

Figure 2-2. Slider-crank configuration with parameters L_1, L_2, x, and θ.

A typical slider-crank configuration is shown in Fig. 2-2. The relationship between the actuator (linear) displacement and crank angle is given by the law of cosines:

$$x^2 = L_1^2 + L_2^2 - 2L_1 L_2 \cos\theta \tag{1}$$

where L_1 and L_2 are the two fixed-length segments of the slider-crank, θ is the angle between those segments, and x (which represents the actuator length) can vary between a fully contracted state, x_{min}, and a fully extended state, x_{max}. The relationship between slider force and crank torque can be obtained by assuming no internal losses (i.e., method of virtual work) as follows:

$$\tau = F\frac{dx}{d\theta} = \frac{F L_1 L_2 \sin\theta}{\sqrt{L_1^2 + L_2^2 - 2L_1 L_2 \cos\theta}} \tag{2}$$

For the pneumatic actuator, the force F is given by the product of actuator diameter and operating pressure, which in this case is 2 MPa (300 psig). Based on these relationships, a multi-tiered exhaustive search minimization was conducted to find a minimum volume actuator that could provide the requisite range of motion and torque/angle phase space as follows:

For a given actuator diameter and stroke length (which determine x_{min} and x_{max}), combinations of L_1 and L_2 were determined, based on equation (1), that provide the requisite range of motion. Note that the actuator diameter influence is not intuitive, but does affect the cylinder length as a function of stroke. For these combinations, the peak torque was computed, based on maximizing equation (2) as a function of θ. The optimal solution was the one that provided the requisite peak torque and secondly minimized the angle between the mechanism peak torque and the angle at which it occurs during gait, and, if necessary, additionally minimized the length L_1.

The joint specifications and ranges considered for L_1 and L_2 are given in Table 2-1, the actuator sizes considered are given in Table 2-2, and finally the optimized solution is given in Table 2-3. Note that the ankle actuator can supply only 76% of the torque required for fast walking by a 75 kg user. Though solutions did exist for the full ankle torque, these solutions placed the geometry envelope of the prototype outside of the typical human anthropomorphic envelope. As such, it was decided to trade the peak torque capability of the ankle in order to limit the size of the ankle actuator and the L_1 dimension in order to stay within the volumetric envelope of the anthropomorphic norm and reduce overall weight of the device. Experimental trials with the device will determine whether or not this was a worthwhile design trade-off. The torque/angle phase space of the resulting knee and ankle actuator configurations are shown graphically in Figs. 2-3 and 2-4, along with the data for a 75 kg normal human for slow and fast cadence and stair climbing Winter (1988), Winter and Sienko (1988), Nadeau et al. (2003).

Table 2-1. Parameters used for optimization of actuator size and configuration.

Parameter	Values for Knee Actuator	Values for Ankle Actuator
Peak Kinematic Torque Required	86 Nm	130 Nm
Angle at Peak Kinematic Torque	25°	10°
Minimum Range of Motion	110°	65°
Range of L_1	0.001 – 3.16 cm	0.001 – 3.16 cm
Range of L_2	0.001 – 30 cm	0.001 – 30 cm

Table 2-2. Actuator parameters considered in optimization.

Actuator Diameters	7/8”, 17/16”, 1.25”, 1.5”, 1.75”, 2”
Actuator Stroke Length	0.25” – 6”
Maximum Operating Pressure	2 MPa (300 psig)

Table 2-3. Results of parameter optimization of actuator size and configuration.

Parameter	Values for Knee Actuator	Values for Ankle Actuator
L_1	4.3 cm	5.1 cm
L_2	28.8 cm	26.3 cm
Range of Actuator Motion	125°	87°
Actuator Diameter	1.5”	1.5”
Actuator Stroke	3”	2.75”
Peak Actuator Torque	102 Nm	119 Nm
Supplied Actuator Torque at Angle of Peak Kinematic Torque	86 Nm	100 Nm

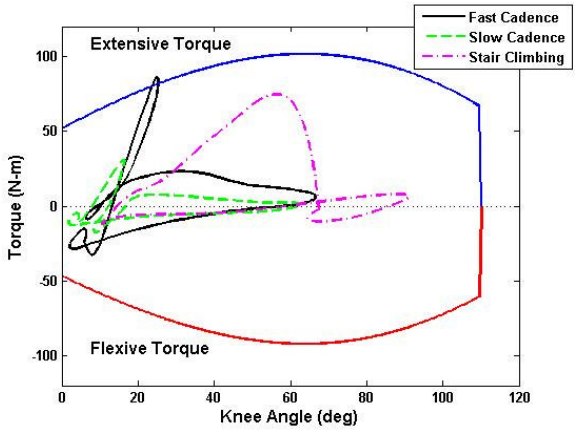

Figure 2-3. Knee joint angle versus torque during one power cycle for typical 75 kg normal subject and theoretical active knee joint prosthetic operating at 2 MPa (300 psig).

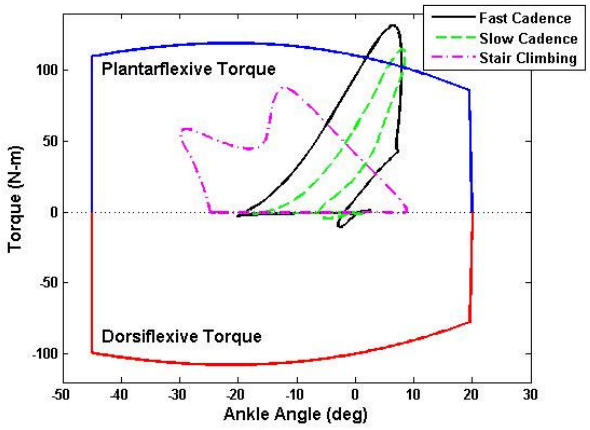

Figure 2-4. Ankle joint angle versus torque during one power cycle for typical 75 kg normal subject Winter and theoretical active ankle joint prosthetic operating at 2 MPa (300 psig).

4. Prosthesis Design

Figures 2-6 and 2-7 show a labeled solid model and a photograph, respectively, of the assembled prosthesis prototype. The device incorporates double-acting pneumatic actuators (Bimba model 17-3-DP for the knee joint, model 17-2.75-DP for the ankle). Operating at 300 psig, the actuators are capable of producing 510 lbf of outward axial force, and 465 lbf on the return. It should be noted that heavier users could be accommodated by increasing the operating pressure (e.g., up to 500 psig, which would accommodate joint torques required for a 125 kg user). Flow to the cylinders is controlled by custom four-way servovalves, shown in Fig. 2-5. The sensor package for the prosthesis includes joint torque and position sensors along with a custom 3-axis socket load cell, described in detail in Section 5, which measures the axial force, sagittal plane moment, and frontal plane moment at the interface between the prosthesis and socket. The torque at each joint is measured via uniaxial load cells (Honeywell Sensotec model 11) located in line with the actuator piston rods. The ankle and knee joints each contain integrated joint motion sensors (ETI Systems model SP12S precision potentiometer). A potentiometer was chosen

as a joint angle sensor rather than an optical encoder to provide high-resolution absolute position measurement in a small package size. The potentiometers lie inside a pair of Teflon/porous bronze composite dry bearings (Garlock model DU) within each joint, as shown in the cross section of Fig. 2-8. Figure 2-9 shows the range of motion of the knee and ankle joints, while Fig. 2-10 shows the geometric envelope of the active knee and ankle prosthesis relative to the human leg.

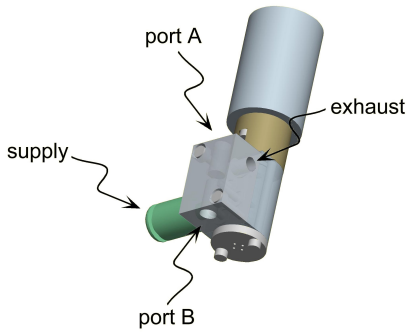

Figure 2-5. Rotary 4-way servovalve for use in prosthesis.

Figure 2-6. Major components of power-tethered prototype.

Figure 2-7. Actual tethered transfemoral prosthesis prototype.

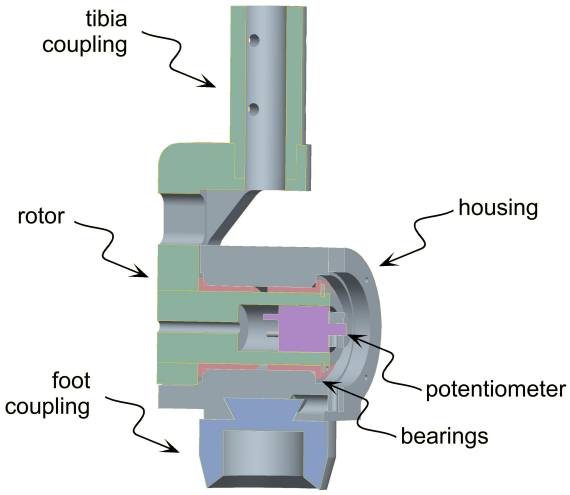

Figure 2-8. Section view of ankle joint, showing integrated potentiometer (i.e., joint angle sensor).

Figure 2-9. Range of motion of active knee and ankle prosthesis simulator. LEFT: Knee and ankle joints at zero angular displacement; MIDDLE: Knee fully flexed (110°) and ankle fully plantarflexed (45°); RIGHT: Knee fully extended (0°) and ankle fully dorsiflexed (20°).

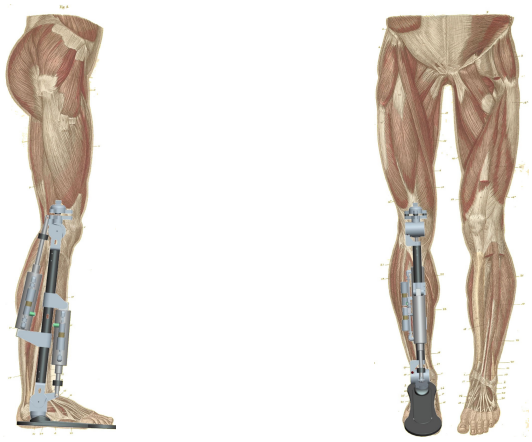

Figure 2-10. Sagittal and frontal geometry of the active knee and ankle prosthesis relative to an anthropomorphic norm.

The structural components of the prosthesis were designed to withstand a 2224 N (500 lbf) load and maximum actuator joint torques using ProE Mechanica finite element analysis (FEA) software to verify safe stress conditions. The results of these analyses, depicted in Figs. 2-11 through 2-14, indicate that 7075-T6 aluminum, which has a minimum yield strength in excess of 500 MPa, provides a factor of safety between 1.7 and 3.7 for the design conditions.

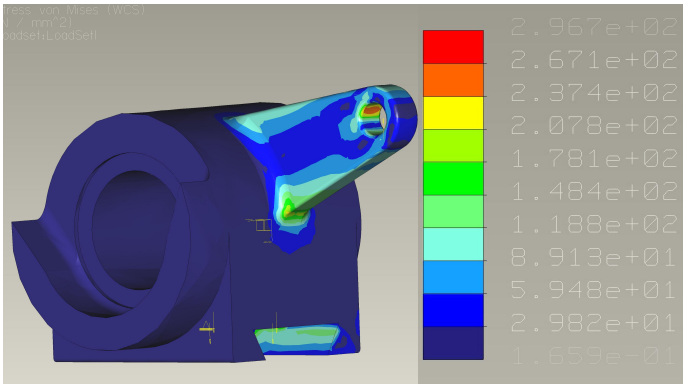

Figure 2-11. ProE Mechanica finite element analysis of ankle joint housing actuator attachment point subjected to 2224 N (500 lbf) vertical force. Maximum von mises stress is 297 Mpa.

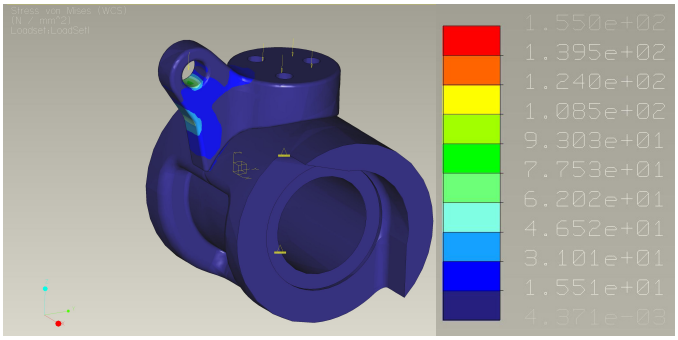

Figure 2-12. ProE Mechanica finite element analysis of knee joint housing actuator attachment point subjected to 2224 N (500 lbf) downward vertical force and 1000 N downward vertical force on load cell attachment point. Maximum von mises stress is 155 Mpa.

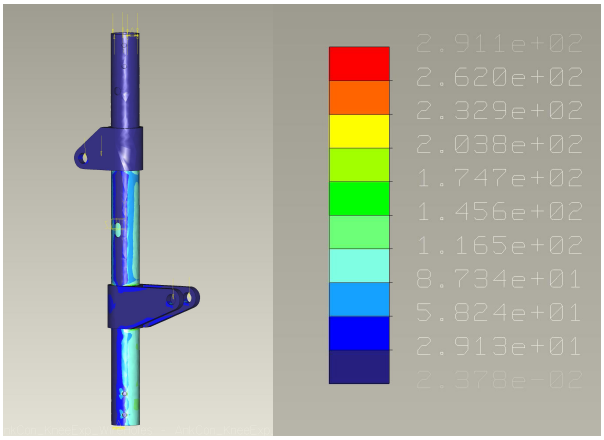

Figure 2-13. ProE Mechanica finite element analysis of tibial tube subjected to 2224 N compressive force and actuator attachment clamps subjected to 2224 N (500 lbf) downward vertical force. Maximum von mises stress is 291 Mpa.

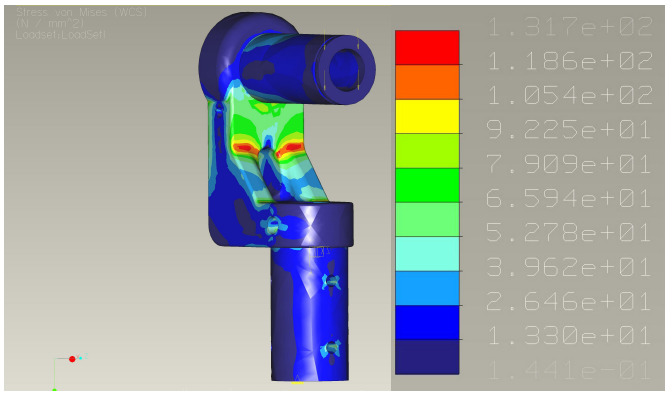

Figure 2-14. ProE Mechanica finite element analysis tibia coupling and rotor subjected to 1000 N compressive force at the free end of the rotor. Maximum von mises stress is 132 Mpa.

The active prosthesis was designed to fit a broad range of different sized persons, ranging from two standard deviations below the female norm in length, up to two standard deviations above the male norm in length based on data from Gorden et al. (1988). The tibial length is varied by changing the single structural (tibia) tube and the clamping supports for the actuators allow for adjustment to achieve the recommended spacing as dictated by the kinematic configuration optimization. The foot is a low profile prosthetic foot (Otto Bock Lo Rider), with typical sizes available. Additionally, the ankle joint and the 3-axis socket load cell incorporate standard pyramid connectors for coupling the prosthesis to the feet and socket, thus enabling a high degree of adjustment in the knee and ankle alignment, as is standard in transfemoral prostheses. Based on actual prosthesis weight and combined with the use of an Otto Bock Lo Rider foot 0.37 kg (0.8 lb), the total weight of the transfemoral prosthesis with pyramid connectors is 2.65 kg (5.8 lb), which is within the normal and acceptable range for transfemoral prostheses and less then a comparable normal limb segment Clauser et al. (1969).

5. Load Cell Design

As previously mentioned, the interaction forces and moments between the prosthesis and user must be measured for purposes of prosthesis control and user intent recognition. Such a measurement is most logically made proximal to the knee joint. Based on the data for fast walking and stair climbing, the range of measurement for the load cell was determined to be 1000 N of axial force (i.e., along the socket) and 100 N-m of sagittal and frontal plane moments. Relative to commercially available multi-axis load cells (e.g., ATI and JR3), this combination of force and moment is disproportionately weighted toward the moment measurement. Specifically, commercial multi-axis load cells that met the force requirement had a moment range that was an order of magnitude smaller than the moment requirement. Similarly, commercial multi-axis load cells that met the moment requirement had force ratings an order of magnitude larger than that required, and additionally were much larger than could be realistically implemented in a prosthetic leg. As such, a custom load cell was designed and fabricated. Initially, an effort was made to utilize three commercial uniaxial load cells (Honeywell Sensotec model 11) mounted in a triangle formation to independently measure forces and moments, as depicted in Fig. 2-15. The large moment requirement relative to the force range, and the fact that the package diameter was restricted by the diameter of a leg, required the use of 2225 N (500 lbf) uniaxial load cells, such that the total force capacity would be 6675 N (1500 lbf). Since the primary measurement range of interest is an order of magnitude less than this, the sensitivity of this load cell would be unacceptable. As such, a custom three-axis socket load cell was designed.

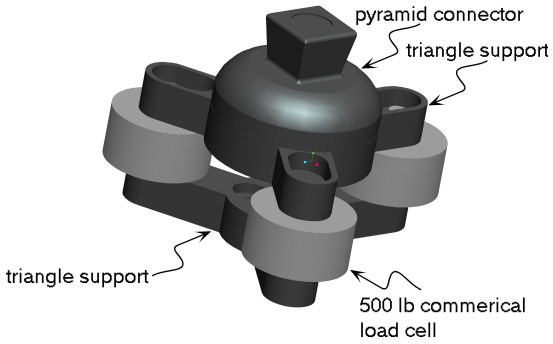

Figure 2-15. Triangle mounted uniaxial commercial load cells not used in final design to due reduced sensitivity to axial force.

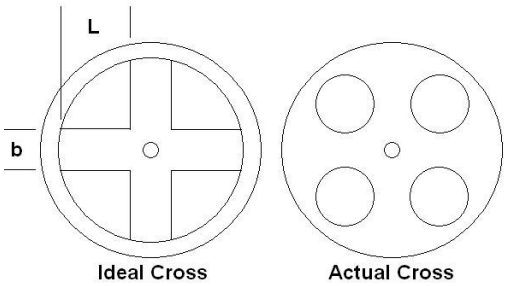

Figure 2-16. Idealized versus actual beam patterns.

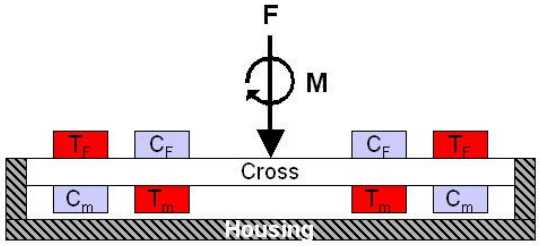

Figure 2-17. Regions of compression (C) and tension (T) in a sectional view of the single cross for an applied force, F, and moment, M. Subscripts denote loading responsible for the compression and tension.

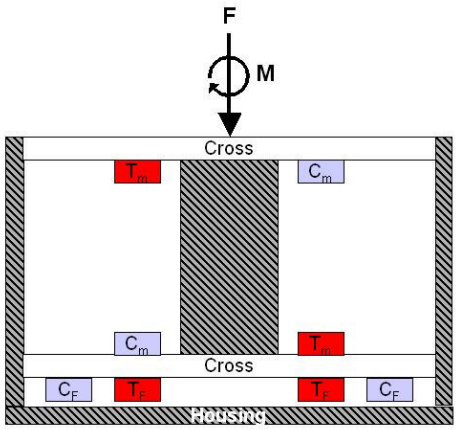

Figure 2-18. Regions of compression (C) and tension (T) in a sectional view of the double cross for an applied force, F, and moment, M. Subscripts denote loading responsible for the compression and tension.

The basis of the socket load cell design is a crossed beam, as depicted in Fig. 2-16. The initial design utilized a single crossed beam, which measures the force and moments via the relative regions of tension and compression as indicated in Fig. 2-17. Based on assumptions of linearly elastic, isotropic and homogeneous behavior, the strain due to the axial force can be derived to be:

$$\epsilon_f = \frac{M_b h}{2EI} = \frac{3FL}{2Ebh^2} \tag{3}$$

and the strain due the moment derived to be:

$$\epsilon_m = \frac{M_L h}{2EI} = \frac{3K_L M_L L}{(K_L + K_T)Ebh^2} \tag{4}$$

where,

$$K_L = \frac{8EI(3R^2 + 3RL + L^2)}{L^3} \tag{5}$$

and

$$K_T = \frac{2\beta G b h^3}{L} \tag{6}$$

and

$$M_L = \frac{K_L M_b}{(K_L + K_T)} \tag{7}$$

and

$$M_b = EI\frac{d^2 v}{dx^2} = M\left(\frac{-3L(R-L)}{2(3R^2+3RL+L^2)} + \frac{L^2+6L(R-L)}{8(3R^2+3RL+L^2)}\right) \tag{8}$$

Where *F* is the axial force, *M* is the applied moment, *L* is the length of the beam, *E* is the modulus of elasticity, *b* is the beam width, *h* is the beam thickness, *R* is the length of beam clamped in the center, and *I* is the area moment of inertia given by:

$$I = \frac{bh^3}{12} \tag{9}$$

The objective of the design with a single cross is to develop strains of similar magnitudes (e.g., approximately 1000 microstrain for metal foil gages) for a desired applied force and moment. For the range of forces and moments of interest in this application (1000 N and 100 N-m, respectively), and for the allowable geometric envelope of the load cell, no satisfactory solution could be obtained (i.e., sensitivity to applied moments was significantly greater than sensitivity to applied forces).

Rather than use a single cross configuration, which fundamentally utilizes bending to measure both the applied force and moment, a double cross design was developed in order to effectively change the fundamental mechanism by which the moment was measured. Specifically, by utilizing a pair of crosses as

shown in Fig. 2-18, the moment is counteracted by a force couple, which loads the beams in tension and compression, while (like the single cross configuration) the force is counteracted by loading the beams in bending. By introducing fundamentally different mechanisms of loading between the force and moment measurement, the relative geometry of the cross could be manipulated to generate similar strain sensitivity.

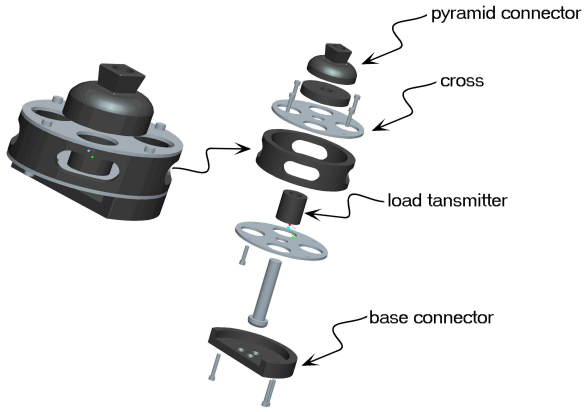

Figure 2-19. Double cross in assembled and exploded view showing the configuration of the two approximated crosses.

The double cross design, which is shown in Fig. 2-19, consists of two single crosses separated by a distance and rigidly held together by a housing on the outside and load transmitter in the center. This introduces a levering action, via the load transmitter, between the crosses when a moment is applied. For a given applied moment, the strain in the beams can be calculated as:

$$\epsilon_m = \frac{F}{AE} = \frac{M}{tbhE} \tag{10}$$

where,

$$F = \frac{M}{t} \tag{11}$$

and

$$A = b\,h \tag{12}$$

Where ε_m is the strain resulting from the applied moment, M, t is the separation between the plates, *b* is the width of the beam, *h* is the thickness of the plates, and *E* is the modulus. As the distance increases between the two plates, the forces in each of the supporting beams decreases. The distance between the plates is used to bring the resulting force and moment strains on the same order and within the measurable range of a strain gage. The double cross still utilizes beam bending to measure the force the same manner as that used for the single cross design, however, the force is now distributed via four beams, instead of two (i.e., strain given by equation (3), although a factor of two less for a given force).

Based on appropriate versions of equations (3) and (10), the double load cell was optimized using a recursive MATLAB program code to optimize for the smallest overall device size. The optimization constraints were to have the sum of strains be less than 1500 microstrain, have the strains, ε_f and ε_m, be on the same order, and search for the minimum load cell volume that meets the criteria. The results of the optimization for the load cell design are listed in Table 2-4. The resulting strains were then verified via a ProE Mechanica finite element analysis, the results of which are shown in Figs. 2-20 and 2-21.

Table 2-4. Results of parameter optimization of 3-axis load cell dimensions.

Parameter	Symbol	Value
Length of Beam	L	20 mm
Width of Beam	b	16 mm
Height of Beam	h	2 mm
Plate Separation	t	23 mm
Modulus of Plate Material	E	193 Gpa (301 stainless steel)
Predicted strain from Force	ε_f	610 με
Predicted strain from Moment	ε_m	870 με

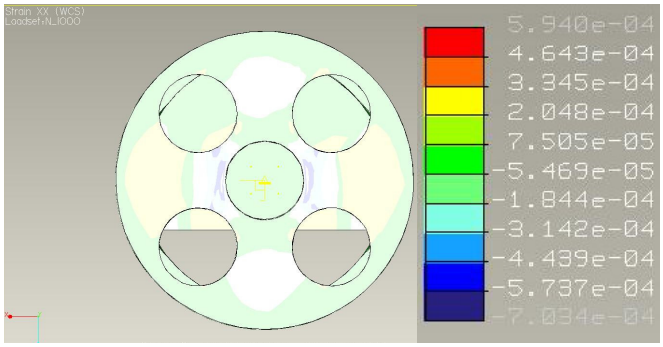

Figure 2-20. ProE Mechanica analysis of 3-axis socket load cell subjected to 1000 N compressive axial force. Peak microstrain in the area location of the stain gages is 400 με.

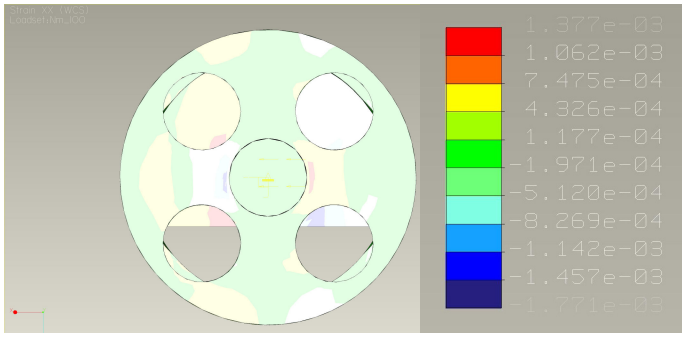

Figure 2-21. ProE Mechanica analysis of 3-axis socket load cell subjected to 100 Nm moment in the frontal plane. Peak microstrain in the location of the stain gages is 700 με.

The device was fabricated using the actual cross design as depicted in Fig. 2-16. Strain gages (Vishay Micromeasurements EA-06-125AC-350) were applied in a pattern depicted by Fig. 18. The final assembled and wired device, which can be seen in Fig. 6, weighs 360 g. The calibration of the load cell was two-fold. First, reference loads were placed directly on top of the load cell. In the second, depicted in Fig. 2-22, reference masses were hung from an arm inline with cross beams at varying distances from the load cell to impart a moment onto the load cell with varying forces, and forces onto the load cell with varying moments. The voltage readings from each of the three bridges were taken for all calibration points. A least squares method was used to calculate coefficients of a transformation matrix between the vector of applied forces and moments and the vector of measured voltage output from the three bridges based on a fifth-order polynomial fit using MATLAB. The results of the calibration are shown in Figs. 2-23, 2-24 and 2-25. In these figures, the 45° line represents the zero-error solution where applied load is equal to the calculated load. The relatively small error that exists in the calibration is due to (mechanical) cross talk between the applied forces and moments.

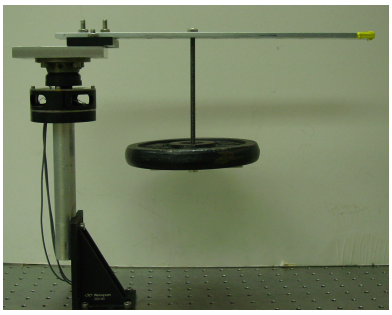

Figure 2-22. Calibration setup of 3-axis socket load cell in moment calibration configuration.

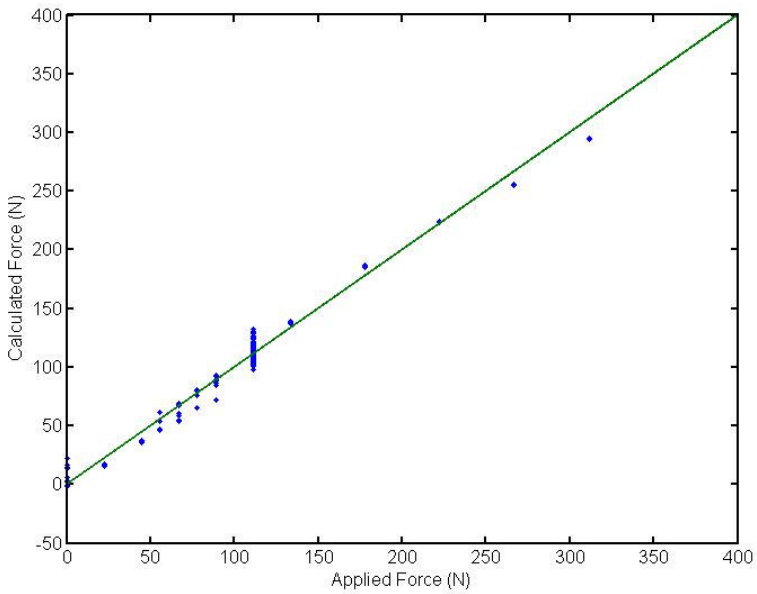

Figure 2-23. Applied versus calculated force, where line represents ideal solution where applied is equal to calculated.

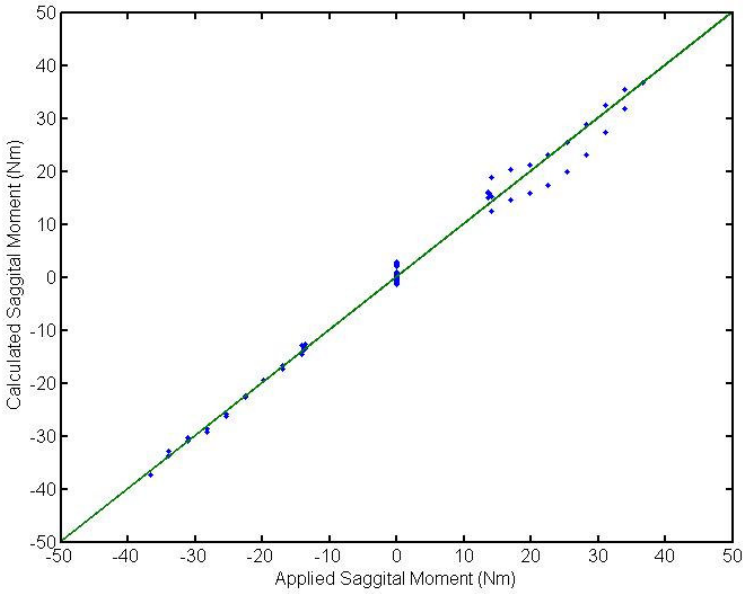

Figure 2-24. Applied versus calculated sagittal moment, where line represents ideal solution where applied is equal to calculated.

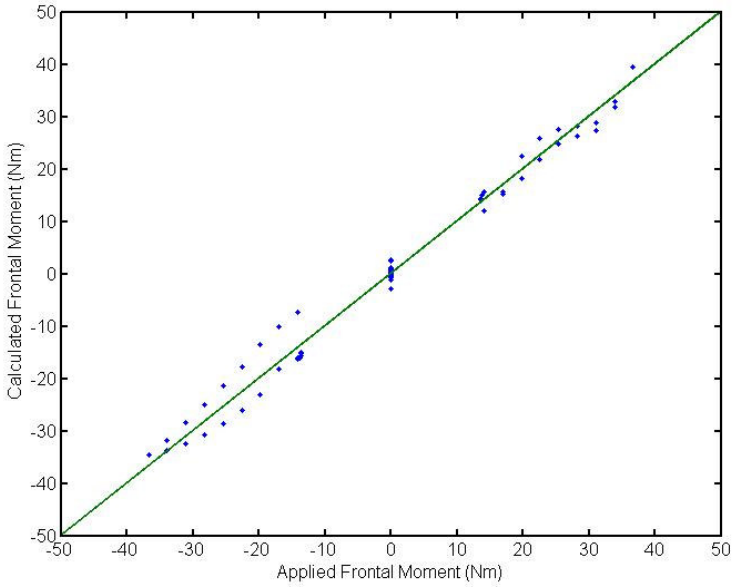

Figure 2-25. Applied versus calculated frontal moment, where line represents ideal solution where applied is equal to calculated.

6. Able-Body Testing Adaptor

Development and testing of the prosthesis controller will be facilitated by the use of an able-boded testing adaptor, which will enable extensive in-house testing and validation of the prosthesis prior to any transfemoral amputee participant involvement. The testing adaptor will enable a healthy subject to wear and walk with the prosthesis prototype. Gait trials with the testing adaptor will be used to thoroughly evaluate the performance, safety, and functionality of the fully controlled prosthesis prior to any transfemoral participant involvement. Design of the able-bodied testing adaptor is shown in Fig. 2-26. As shown in the figure, the adaptor consists of a commercial adjustable locking knee immobilizer (KneeRANGER-Universal Hinged Knee Brace) with an adaptor bracket that transfers load from the subject to the prosthesis. Figure 2-27 shows for comparison both a transfemoral amputee with the prosthesis and a healthy subject with adaptor/prosthesis. Since the prosthesis remains lateral to the immobilized leg of the healthy subject, the

adaptor will enable replication of transfemoral amputee gait without (geometric) interference from the immobilized leg.

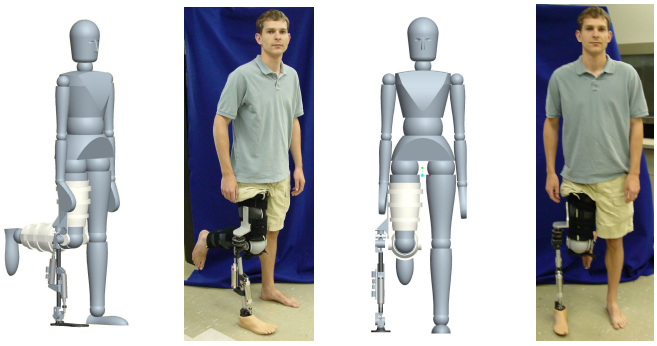

Figure 2-26. Design of the able-bodied testing adaptor, which will enable development, testing, and evaluation of the proposed prosthesis and controllers prior transfemoral amputee participant testing.

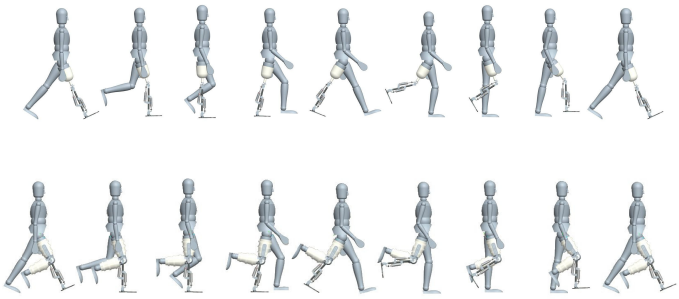

Figure 2-27. Depiction of one stride cycle for transfemoral amputee (above) and healthy subject wearing able-bodied (below).

7. Conclusion

This paper described the design of a tethered pneumatically actuated transfemoral prosthesis. The design requirements were outlined from biomechanical data of unaffected persons and the design was optimized to provide a lightweight device and the structural integrity validated with finite element analysis software. A sensor set to provide full controllability of the prosthesis was integrated into the design.

Among the sensor set is a custom designed three-axis load cell, which measures the forces and moments between the prosthesis and socket. This prosthesis will serve as a laboratory test bed to validate the device performance and develop control algorithms using the able-bodied adaptor. Pending the development of suitable user interface and control approaches, a self-contained version of the prosthesis with on-board power and computing will be developed.

8. References

Clauser CE, McConville JT, Young JM, Weight, volume and center of mass of segments of the human body. AMRL-TR-69-70, Wright Patterson Airforce Base, Dayton, Ohio, 1969.

DeVita, P., Torry M., Glover, K.L., and Speroni, D.L. A Functional Knee Brace Alters Joint Torque and Power Patterns during Walking and Running, Journal of Biomechanics, vol. 29, no. 5, pp. 583-588, 1996.

Donath, M., Proportional EMG Control for Above-Knee Prosthesis', Department of Mechanical Engineering Masters Thesis, MIT, 1974.

Fite, K.B., Mitchell, J., Barth, E.J., and Goldfarb, M. Sliding Mode Control of a Direct-Injection Monopropellant-Powered Arm, *American Control Conference*, pp. 4461-4466, 2004.

Flowers, W.C., A Man-Interactive Simulator System for Above-Knee Prosthetics Studies, Department of Mechanical Engineering PhD Thesis, MIT, 1973.

Flowers, W.C., and Mann, R.W., Electrohydraulic knee-torque controller for a prosthesis simulator. ASME Journal of Biomechanical Engineering, vol. 99, no. 4, pp. 3-8, 1977.

Goldfarb, M., Barth, E.J., Gogola, M.A. and Wehrmeyer, J.A., Design and Energetic Characterization of a Liquid-Propellant-Powered Actuator for Self-Powered Robots. *IEEE/ASME Transactions on Mechatronics*, vol. 8, no. 2, pp. 254-262, 2003.

Gordon, CC, B. Bradtmiller, T. Churchill, C.E. Clauser, J.T. McConville, I. Tebbetts and R. Walker. 1988 Anthropometric Survey of US Army Personnel: Methods and Summary Statistics. Technical Report NATICK/TR-89/044, U.S. Army Natick Research, Development and Engineering Center, Natick, MA, 1989.

Grimes, D. L., Flowers, W. C., and Donath, M., Feasibility of an active control scheme for above knee

prostheses. ASME Journal of Biomechanical Engineering, vol. 99, no. 4, pp. 215-221, 1977.

Grimes, D. L., An Active Multi-Mode Above Knee Prosthesis Controller. Department of Mechanical Engineering PhD Thesis, MIT, 1979.

Jacobs, R., Bobbert, M.F., van Ingen Schenau, G.J., Mechanical output from individual muscles during explosive leg extensions: the role of biarticular muscles. Journal of Biomechanics, vol. 29, no. 4, pp. 513-523, 1996.

Klute, G.K., Czerniecki, J., Hannaford, B., Development of Powered Prosthetic Lower Limb, Proceedings of the First National Meeting, Veterans Affairs Rehabilitation Research and Development Service, 1998.

Klute, G.K., Czerniecki, J., Hannaford, B., Muscle-Like Pneumatic Actuators for Below-Knee Prostheses, Proceedings the Seventh International Conference on New Actuators, pp. 289-292, 2000.

Nadeau, S., McFadyen, B.J., and Malouin, F. Frontal and sagittal plane analyses of the stair climbing task in healthy adults aged over 40 years: What are the challenges compared to level walking? Clinical Biomechanics, vol. 18, no. 10, pp. 950-959, 2003.

Nagano, A., Ishige, Y., and Fukashiro, S., Comparison of new approaches to estimate mechanical output of individual joints in vertical jumps. Journal of Biomechanics, vol. 31, no. 10, pp. 951-955, 1998.

Popovic, D. and Schwirtlich, L., Belgrade active A/K prosthesis, in de Vries, J. (Ed.), Electrophysiological Kinesiology, Interm. Congress Ser. No. 804, Excerpta Medica, Amsterdam, The Netherlands, pp. 337–343, 1998.

Prilutsky, B.I., Petrova, L.N., and Raitsin, L.M., Comparison of mechanical energy expenditure of joint moments and muscle forces during human locomotion. Journal of Biomechanics, vol. 29, no. 4, pp. 405-415, 1996.

Riener, R., Rabuffetti, M., and Frigo, C., Joint powers in stair climbing at different slopes. Proceedings of the IEEE International Conference on Engineering in Medicine and Biology, vol. 1, p. 530, 1999.

Shields, B., Fite, K., and Goldfarb, M., Control of a Direct Injection Liquid Fueled Actuator, Proceedings of the ASME International Mechanical Engineering Congress and Exposition, IMECE2004-59442, 2004.

Shields, B., and Goldfarb, M., Design and Energetic Characterization of a Solenoid Injected Liquid Monopropellant Powered Actuator for Self-Powered Robots, accepted for the 2005 IEEE International Conference on Robotics and Automation, 2005.

Stein, J.L., Design Issues in the Stance Phase Control of Above-Knee Prostheses. Department of Mechanical Engineering PhD Thesis, MIT, 1983.

Stein, J.L., and Flowers, W.C., Stance phase control of above-knee prostheses: knee control versus SACH

foot design. Journal of Biomechanics, vol. 20, no. 1, pp. 19-28, 1987.

Waters, R., Perry, J., Antonelli, D., and Hislop, H., Energy cost of walking amputees: the influence of level of amputation. J. Bone and Joint Surgery. 58A, 42–46, 1976.

Winter, D. A. and Sienko, S. E., Biomechanics of below-knee amputee gait. J. Biomechanics. 21, 361–367, 1988.

Winter, D.A., The biomechanics and motor control of human gait: normal, elderly and pathological, University of Waterloo Press, 2nd ed., 1991.

CHAPTER III

ADDENDUM TO MANUSCRIPT I

1. Prosthesis Design

Appendix A comprises of parts list for the prosthesis, socket load cell and able-bodied adaptor. The focal point of the design of a powered prosthesis is the kinematic configuration of the actuators. The actuators in this design is what provides the paradigm shift from previous prosthesis designs and the actuators must be able to provide the necessary torques at the knee and ankle in order to provide the increased functionality promised. The basic design crux of the kinematic configuration of the actuators is to provide the greatest amount of torque capability in the smallest volumetric envelope. In order to find a solution two approaches were explored; analytical and numerical. The analytical solution did not lead to a finite solution due to complications in the nonlinear geometry. Instead, a numerical approach was chosen and used in the final design of the leg. The numerical method used is described in Chapter 2.3 and the Matlab M-file code is presented in Appendix B.

2. Socket Load Cell

The calibration graphs presented in Chapter 2.5 for the socket load cell were obtained using a fifth order linear least squares fit to the raw data. Using the standard definition for least squares:

$$\theta = \left(\Phi^T \cdot \Phi\right)^{-1} \cdot Y \tag{1}$$

where,

$$\Phi = \begin{pmatrix} F \\ F^2 \\ F^3 \\ F^4 \\ F^5 \\ M_F \\ M_F^2 \\ M_F^3 \\ M_F^4 \\ M_F^5 \\ M_S \\ M_S^2 \\ M_S^3 \\ M_S^4 \\ M_S^5 \end{pmatrix} \tag{2}$$

and

$$Y = \begin{pmatrix} F & M_F & M_S \end{pmatrix} \tag{3}$$

Using the calibration data in the linear least squares equation the following matrix results:

$$\theta = \begin{pmatrix} 128.9451 & -7.0311 & 1.7243 \\ 107.8560 & 28.6214 & -12.1171 \\ 64.1953 & -58.1033 & 25.9484 \\ -167.1647 & 50.5421 & -18.7935 \\ 60.4584 & -14.4553 & 4.3797 \\ -102.9251 & 14.6247 & -1.6182 \\ -56.6244 & 2.5802 & -2.7663 \\ -49.5004 & 9.5874 & -0.6774 \\ -8.3461 & 6.6598 & -0.1948 \\ 2.0407 & 2.2391 & -0.3181 \\ -12.7130 & 0.3288 & 6.7424 \\ -17.6753 & -0.2394 & -0.7462 \\ 4.7048 & -0.3485 & 1.0689 \\ 1.7970 & 0.1025 & 0.1106 \\ -0.3911 & 0.0233 & -0.0445 \end{pmatrix} \quad (4)$$

As demonstrated in the calibration results presented in Chapter 2.5, the resulting matrix, Equation (4), provides good correlation over the calibrated range of torques and forces. Outside of this range the load cells accuracy decreases dramatically. Future work with this load cell, requires calibration over the entire range of operation in order to provide accurate results.

CHAPTER IV

MANUSCRIPT II: DESIGN AND CONTROL OF A POWERED TRANSFEMORAL PROSTHESIS

Frank Sup, Amit Bohara and Michael Goldfarb

Department of Mechanical Engineering

Vanderbilt University

Nashville, TN 37235

Submitted as a Full Paper to the

International Journal of Robotics Research

for consideration in the special issue on

Machines for Human Assistance and Augmentation

1. Abstract

The paper describes the design and control of a transfemoral prosthesis with powered knee and ankle joints. The initial prototype is a pneumatically-actuated powered-tethered device, which is intended to serve as a laboratory test bed for a subsequent self-powered version. After the design of the prosthesis is described, a gait controller is proposed based on the use of passive impedance functions that coordinates the motion of the prosthesis and user during level walking. The control approach is implemented on the prosthesis prototype, and experimental results are shown that demonstrate the effectiveness of the active prosthesis and control approach in restoring fully powered level walking to the user.

2. Introduction

2.1 Motivation

Despite significant technological advances over the past decade, such as the introduction of microcomputer-modulated damping during swing, commercial transfemoral prostheses remain limited to energetically passive devices. That is, the joints of the prostheses can either store or dissipate energy, but cannot provide net power over a gait cycle. The inability to deliver joint power significantly impairs the ability of these prostheses to restore many locomotive functions, including walking up stairs and slopes, running, and jumping, all of which require significant net positive power at the knee joint, ankle joint, or both (Winter and Sienko 1988, Nadeau et al. 2003, Riener et al. 1999, Prilutsky et al. 1996, DeVita et al. 1996, Nagano et al. 1998, Jacobs et al. 1996). Further, although less obvious, even biomechanically normal walking requires positive power output at the knee joint and significant net positive power output at the ankle joint (Winter, 1991). Transfemoral amputees walking with passive prostheses have been shown to expend up

to 60% more metabolic energy relative to healthy subjects during level walking (Waters et al. 1976) and exert as much as three times the affected-side hip power and torque (Winter 1991), presumably due to the absence of powered joints. A prosthesis with the capacity to deliver power at the knee and ankle joints would presumably address these deficiencies, and would additionally enable the restoration of biomechanically normal locomotion. Such a prosthesis, however, would require 1) power generation capabilities comparable to an actual limb and 2) a control framework for generating required joint torques for locomotion while ensuring stable and coordinated interaction with the user and the environment. This paper describes the authors' progress to date in pursuing both of these goals. Specifically, section 2 presents the current prosthesis prototype design and discusses the means by which the authors intend to convert this to a self-powered version; section 3 describes the control approach, and section 4 presents experimental results that validate the hardware and control approach.

2.2 Background

Though the authors are not aware of any prior work on the development of a powered knee and ankle prosthesis, prior work does exist on the development of powered knee transfemoral prostheses and powered ankle transtibial prostheses. Regarding the former, Flowers (1973), Donath (1974), Flowers and Mann (1977), Grimes et al. (1977), Grimes (1979), Stein (1983), and Stein and Flowers (1988) developed a tethered electrohydraulic transfemoral prosthesis that consisted of a hydraulically actuated knee joint tethered to a hydraulic power source and off-board electronics and computation. They subsequently developed an "echo control" scheme for gait control, as described by Grimes et al. (1977), in which a modified knee trajectory from the sound leg is played back on the contralateral side. In addition to this prior

work directed by Flowers, other groups have also investigated powered knee joints for transfemoral prostheses. Specifically, Popovic and Schwirtlich (1988) report the development of a battery-powered active knee joint actuated by DC motors, together with a finite state knee controller that utilizes a robust position tracking control algorithm for gait control (Popovic et. al., 1995). With regard to powered ankle joints, Klute et al. (1998, 2000) describe the design of an active ankle joint using pneumatic McKibben actuators, although gait control algorithms were not described. Au et al. (2005) assessed the feasibility of an EMG based position control approach for a transtibial prosthesis. Finally, though no published literature exists, Ossur, a major prosthetics company based in Iceland, has announced the development of both a powered knee and a self-adjusting ankle. The latter, called the "Proprio Foot," is not a true powered ankle, since it does not contribute power to gait, but rather is used to quasistatically adjust the angle of the ankle to better accommodate sitting and slopes. The powered knee, called the "Power Knee," utilizes an echo control approach similar to the one described by Grimes et al. (1977).

Unlike any prior work, this paper describes a prosthesis design that consists of both a powered knee and ankle, and describes a method of control that enables natural, stable interaction between the user and the powered prosthesis. The control approach is implemented on the prosthesis prototype fit to a user, and experimentally shown to provide powered level walking representative of normal gait.

3. Prosthesis Design

One of the most significant challenges in the development of a powered lower limb prosthesis is providing self-powered actuation capabilities comparable to biological systems. State-of-the-art power supply and actuation technology such as battery/DC motor combinations suffer from low energy density of

the power source (i.e., heavy batteries for a given amount of energy), low actuator force/torque density, and low actuator power density (i.e., heavy motor/gearhead packages for a given amount of force or torque and power output), all relative to the human musculoskeletal system. Recent advances in power supply and actuation for self-powered robots, such as the liquid-fueled approaches described by Goldfarb et al. 2003, Shields et al. 2006, Fite et al. 2006, and Fite and Goldfarb 2006, offer the potential of significantly improved energetic characteristics relative to battery/DC motor combinations, and thus bring the potential of a powered lower limb prosthesis to the near horizon. Specifically, the aforementioned publications describe pneumatic-type actuators, which are powered by the reaction products of a catalytically decomposed liquid monopropellant. The proposed approach has been experimentally shown to provide an energetic figure of merit an order of magnitude greater than state-of-the-art batteries and motors (Shields et al. 2006, Fite and Goldfarb 2006). Rather than construct a self-powered version directly, the authors have developed a power-tethered version of the prosthesis, which enables laboratory-based controller development and prosthesis testing. The self-powered version should be nearly identical to the power-tethered version, but will include an on-board propellant cartridge and catalyst pack in place of the pneumatic tether. This section describes the design of the power-tethered pneumatically actuated prosthesis prototype.

3.1 Design Specifications

The active joint torque specifications were based on the torque/angle phase space required for a 75 kg user for fast walking and stair climbing, as derived from body-mass-normalized data from Winter (1991) and Nadeau et al. (2003), respectively. Minimum range of motion was determined to be 110° of flexion for the knee, and 45° of planterflexion and 20° of dorsiflexion for the ankle. Based on these desired specifications,

the joint actuators and their respective kinematic configurations were selected via a design optimization to minimize the actuator volume that would achieve the desired phase space. The torque/angle phase space for both joints for slow walking, fast walking, and stair climbing (for a 75 kg user), along with the active torque envelope of the prosthesis, are shown in Fig. 1. The optimization resulted in the use of 3.8 cm (1.5 in) diameter cylinders for both knee and ankle joints to accommodate up to a 75 kg user. Note that heavier users could easily be accommodated by slightly increasing the cylinder diameters (e.g., a 4.4 cm, or 1.75 in, cylinder diameter would accommodate up to a 102 kg user).

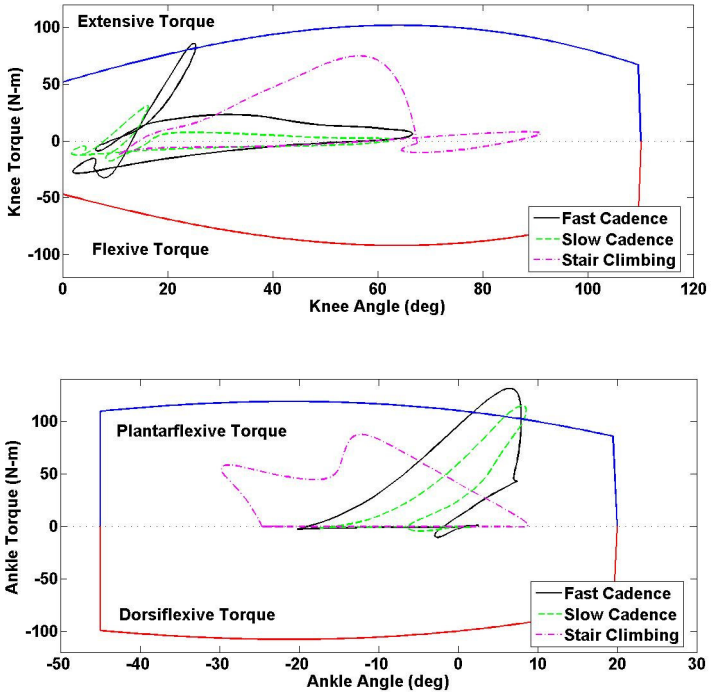

Figure 4-1. Comparison of maximum torque capability of active joints to the torque requirement during various gaits for a 75 kg normal user, based on an operating pressure of 2 MPa (300 psig).

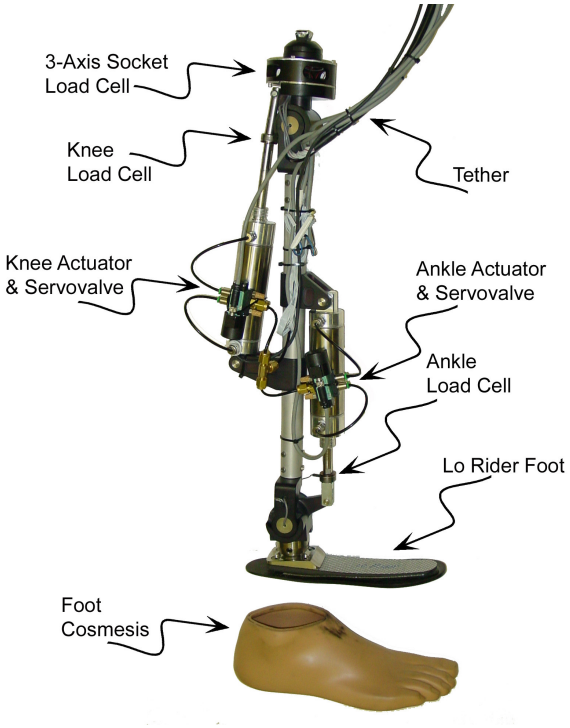

Figure 4-2. The power-tethered prototype.

Figure 2 shows the resulting prosthesis prototype in a labeled photograph. Based on the previously mentioned design optimization, the prosthesis incorporates a 7.6 cm (3 in) stroke, 3.8 cm (1.5 in) bore double-acting pneumatic cylinder (Bimba model 17-3-DP), while the ankle joint incorporates a 7 cm (2.75 in) stroke, 3.8 cm (1.5 in) bore double-acting cylinder (Bimba model 17-2.75-DP). Operating at 2 MPa (300 psig), the actuators are capable of producing 2270 N (510 lbf) of outward axial force, and 2070 N (465 lbf) on the return. Each actuator is controlled via a four-way servovalve (Enfield Technologies LS-V05). Sensors on the prosthesis include cylinder force sensors (which indirectly provide joint torque measurement), joint angle sensors, and a custom 3-axis socket load cell that measures the axial force, sagittal plane moment, and frontal plane moment at the interface between the prosthesis and socket. The cylinder force sensors are uniaxial load cells (Honeywell Sensotec model 11) located in line with the

actuator piston rods. The ankle and knee joint angles are measured via integrated joint motion sensors (ETI Systems model SP12S precision potentiometer), which are located inside the hollow axle and composite plain bearings (Garlock model DU) in each joint. The custom 3-axis load cell, for measurement of the interaction forces and moments between the user and prosthesis, is described subsequently.

The structural components of the prosthesis were designed to withstand a 2224 N (500 lbf) load and maximum actuator joint torques. Safe stress conditions were verified using ProE Mechanica finite element analysis (FEA) software. The results of these analyses indicate that 7075-T6 aluminum, which has a minimum yield strength in excess of 500 MPa, provides a factor of safety between 1.7 and 3.7 for the design conditions.

The powered prosthesis was designed to fit a broad range of different sized persons, ranging from two standard deviations below the female norm in length, up to two standard deviations above the male norm in length based on data from Gorden et al. (1989). The tibial length is varied by changing the single structural (tibia) tube and the clamping supports for the actuators allow for adjustment to achieve the recommended spacing as dictated by the kinematic configuration optimization. The foot is a low profile prosthetic foot (Otto Bock Lo Rider), with typical sizes available. Additionally, the ankle joint and the 3-axis socket load cell incorporate standard pyramid connectors for coupling the prosthesis to the feet and socket, thus enabling a high degree of adjustment in the knee and ankle alignment, as is standard in transfemoral prostheses. Combined with the Otto Bock Lo Rider foot, which weighs 0.37 kg (0.8 lbf), the total weight of the tethered transfemoral prosthesis with pyramid connectors is 2.65 kg (5.8 lbf), which is within the normal and acceptable range for transfemoral prostheses and less than a comparable normal limb segment (Clauser et al., 1969). An untethered version is expected to add an additional 0.9 kg (2 lbf) of weight,

which maintains the prosthesis within an acceptable weight range.

4. Load Cell Design

For purposes of prosthesis control and user intent recognition, the prosthesis incorporates a load cell between the prosthesis and user, which measures the interaction forces and moments. Based on the data presented in Winter (1991) and Nadeau (2003), the required range of measurement for the load cell was determined to be 1000 N of axial force (i.e., along the socket) and 100 N-m of sagittal and frontal plane moments. Relative to commercially available multi-axis load cells (e.g., ATI and JR3), this combination of force and moment is disproportionately weighted toward the moment measurement, and thus would require load cells that are much larger than could be realistically implemented in a prosthetic leg. As such, a custom load cell was designed and fabricated. The basis of the load cell design is a crossed beam spring element, as shown in Fig. 3. The design objective was thus to provide similar strain sensitivities for the axial load and moments (e.g., approximately 1000 microstrain for metal foil gages) for the desired applied force and moment ranges. In order to achieve similar magnitudes, a double cross configuration was developed (as shown in Fig. 4) in order to effectively separate, via a pair of connected crosses, the fundamental mechanisms by which the moment and axial forces are measured. The moment is counteracted by a force couple transmitted by a connecting rod, which loads the beams in tension and compression, while the force is counteracted by loading the beams in bending. The different mechanisms of loading allow the relative geometry of the pair to be manipulated to generate similar strain sensitivity to the desired force and moments. Based on appropriate analytical descriptions of strain, the double load cell was optimized for the smallest overall device size. The resulting strains were then verified via a ProE

Mechanica finite element analysis.

The resulting design, which is shown in Fig. 5, consists of two single crosses separated by a distance and rigidly held together by a housing on the outside and load transmitter in the center. The device was fabricated from a combination of stainless steel and aluminum using the actual cross design as depicted in Fig. 3, and has a total mass of 360 g. The load cell was calibrated utilizing a least squares method to obtain the transformation matrix between the vector of applied forces and moments and the vector of strain gage outputs, based on a fifth-order polynomial. Coupling between load cell axes produces a maximum error of 2.2% of full scale output (FSO) in the axial force measurement, a maximum error of 6.7% FSO in the sagittal moment measurement, and a maximum error of 5.5% FSO in the frontal moment measurement.

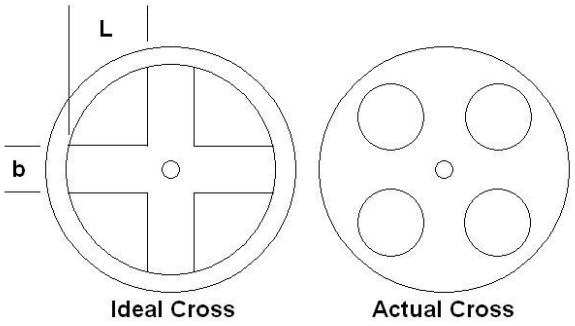

Figure 4-3. Ideal versus actual beam patterns of the socket load cell.

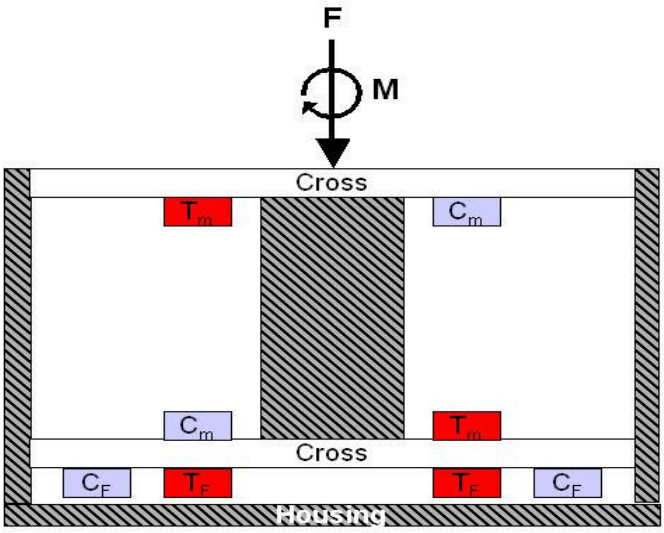

Figure 4-4. Regions of compression (C) and tension (T) in a sectional view of the double cross for an applied force, F, and moment, M for the socket load cell. Subscripts denote loading responsible for the compression and tension.

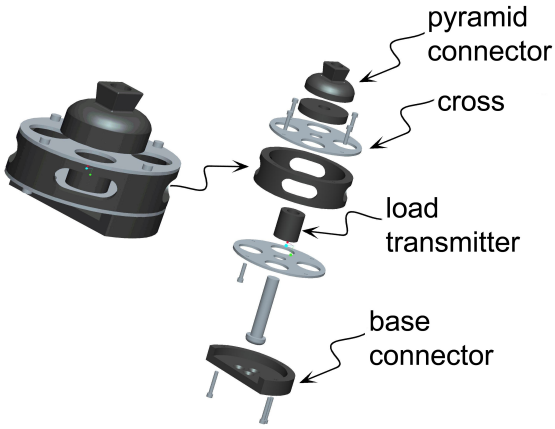

Figure 4-5. Assembled and exploded views of the socket load cell.

5. Gait Control Strategy

The previously described prosthesis is a fully powered two degree-of-freedom robot, capable of significant joint torque and power, which is rigidly attached to a user. As such, the prosthesis necessitates a reliable control framework for generating required joint torques while ensuring stable and coordinated

interaction with the user and the environment.

The overarching approach in all prior work has been to generate a desired joint position trajectory, which by its nature, utilizes the prosthesis as a position source. Such an approach poses several problems for the control of a powered transfemoral prosthesis. First, the desired position trajectories are typically computed based on measurement of the sound side leg trajectory, which 1) restricts the approach to only unilateral amputees, 2) presents the problem of instrumenting the sound side leg, and 3) generally produces an even number of steps, which can present a problem when the user desires an odd number of steps. A subtler yet significant issue with position-based control is that suitable motion tracking requires a high output impedance, which forces the amputee to react to the limb rather than interact with it. Specifically, in order for the prosthesis to dictate the joint trajectory, it must assume a high output impedance (i.e., must be stiff), thus precluding any dynamic interaction with the user and the environment.

Unlike prior works, the approach proposed herein utilizes an impedance-based approach to generate joint torques. Such an approach enables the user to interact with the prosthesis by leveraging its dynamics in a manner similar to normal gait (Mochon and McMahon, 1980), and also generates stable and predictable behavior. The essence of the approach is to characterize the knee and ankle behavior with a series of finite states consisting of passive spring and damper behaviors, wherein energy is delivered to the user by switching between appropriate equilibrium positions (of the virtual springs) in each finite state. In this manner, the prosthesis is guaranteed to be passive within each gait mode, and thus generates power simply by switching between modes. Since the user initiates mode switching, the result is a predictable controller that, barring input from the user, will always default to passive behavior.

5.1 Impedance Characterization of Gait

Based loosely on the notion of impedance control proposed by Hogan (1985), the torque required at each joint during a single stride (i.e., a single period of gait) can be piecewise represented by a series of passive impedance functions. A regression analysis of gait data from Winter (1991) indicates that joint torques can be sufficiently characterized by functions of joint angle and velocity by the simple impedance model

$$\tau = k_1(\theta - \theta_e) + k_2(\theta - \theta_e)^3 + b\dot{\theta} \tag{1}$$

Specifically, the joint torques within each gait mode can be described by the combination of linear and cubic stiffness terms, together with a linear damping term, where k_1 and k_2 characterize the linear and cubic stiffnesses, θ_e is the equilibrium angle, b is the linear damping coefficient, and the angle, θ, and torque, τ, are defined as in Fig. 6. If the coefficients b, k_1, and k_2 are constrained to be positive, then the joint will exponentially converge to a stable equilibrium at $\theta = \theta_e$ and $\dot{\theta} = 0$ within each gait mode. That is, in any given mode, the behavior is passive, and will come to rest at a local equilibrium, thus providing a reliable and predictable behavior for the human user.

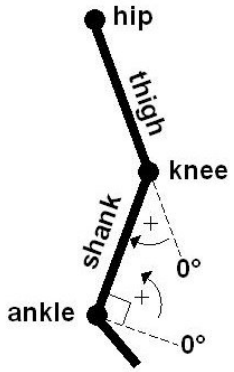

Figure 4-6. Joint angle and torque convention used. Positive torque defined in the direction of increasing angle.

5.2 Gait Modes

As previously discussed, the decomposition of joint behavior into passive segments requires dividing the gait cycle into modes or "finite states," as dictated by their functions and the character of the piecewise segments of the impedance functions previously described. Though the number of modes required is not unique, the switching rules between modes must be well defined and measurable, and the number of modes should be sufficient to provide an accurate representation of normal joint function. One can reasonably assert that the swing and stance phase of gait constitute a minimal set of modes for the proposed approach. Based on least squares regression fitting of gait data (i.e., from Winter, 1991) to equation (1), the authors determined that such fits were improved significantly by further dividing swing and stance into two sub-modes, as shown in Fig. 7, with switching rules as shown in Fig. 8.

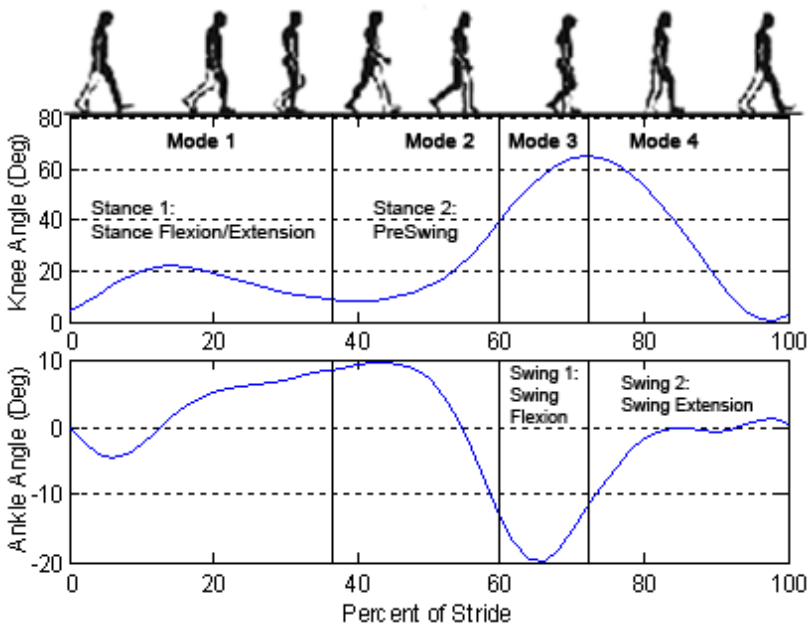

Figure 4-7. Subdivision of normal gait into four functional modes.

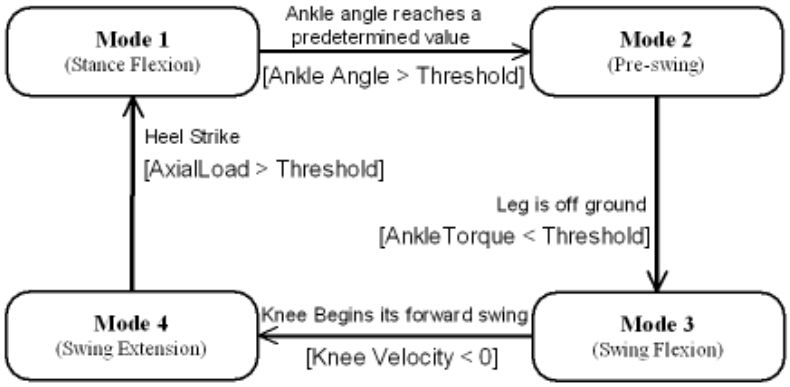

Figure 4-8. A finite state model of normal gait. Each box represents a state and the transition condition between states are specified.

Mode 1 begins with heel strike upon which the knee immediately begins to flex so as to provide impact absorption and begin loading, while the ankle simultaneously plantarflexes to reach foot flat. Both knee and ankle joints have relatively high stiffness during this mode to prevent buckling and allow for appropriate stance knee flexion, since Mode 1 comprises most of the weight bearing functionality. Mode 2 is the push-off phase and begins as the ankle dorsiflexes beyond a given angle (i.e., user's center of mass lies

forward of stance foot). The knee stiffness decreases in this mode to allow knee flexion while the ankle provides a plantarflexive torque for push off. Mode 3 begins as the foot leaves the ground as indicated by the ankle torque load cell and lasts until the knee reaches maximum flexion. Mode 4 is active during the extension of the knee joint (i.e., as the lower leg swings forward) which begins as the knee velocity becomes negative and ends at heel strike (as determined by the 3-axis load cell). In both the swing modes, the ankle torque is small and is represented in the controller as a (relatively) weak spring regulated to a neutral position. The knee is primarily treated as a damper in both swing modes (Mode 3 and 4).

The proposed approach to "impedance modeling" of joint torques was preliminarily validated by utilizing the gait data of a healthy 75 kg subject, as derived from body-mass-normalized data from Winter (1991). Incorporating the four gait modes previously described, along with the motion and torque data for each joint provided by Winter (1991), a constrained least squares optimization was conducted to generate a set of parameters for equation (1) in each mode. The resulting parameter set is listed for each mode in Table 1, and the resulting fit to joint torques is shown graphically in Fig. 9. The fit shown in Fig. 9 clearly indicates that normal joint function can be represented by the use of piecewise passive functions as proposed.

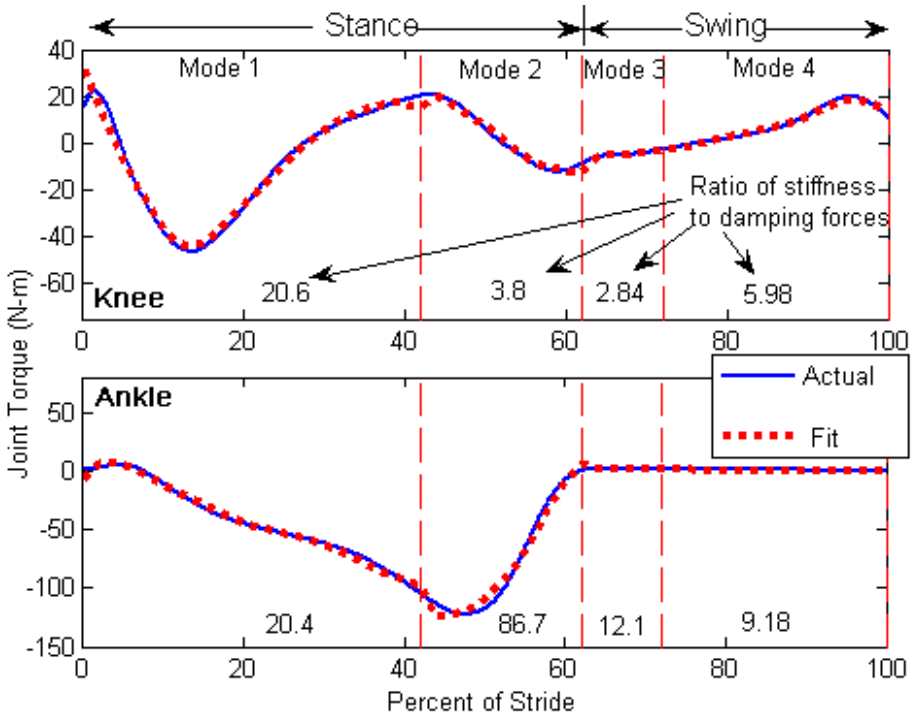

Figure 4-9. Piecewise fitting of knee and ankle torques during normal speed level walk (averaged population data from Winter, 1991 scaled for a 75 kg adult) to a nonlinear spring-damper impedance model. The number shown in each mode represents the mean ratio of the stiffness forces to damping forces predicted by the fit. The vertical lines represent the segmentation of a gait stride into four distinct modes.

Table 4-1. Impedance parameters for prototypical gait (gait data from Winter, 1991).

	Knee Impedance				**Ankle Impedance**			
Mode	k_1 (N.m/deg))	k_2 (N.m/deg^3)	b (N.m.s)	θ_e (deg)	k_1 (N.m/deg))	k_2 (N.m/deg^3)	b (N.m.s)	θ_e (deg)
1	3.78	73e-3	25e-3	12	1.35	25e-3	0.118	-5
2	0	9e-6	30e-3	37	4.50	0	5e-3	-18
3	0	9e-3	16e-3	52	0.04	0	3e-3	23
4	0.093	2e-6	13e-3	44	0.134	0	2e-3	2

6. Experimental Results

The impedance based gait control strategy was implemented on the tethered prosthesis prototype on a

healthy subject using an able-bodied testing adaptor as shown in Fig. 10. The adaptor consists of a commercial adjustable locking knee immobilizer (KneeRANGER-Universal Hinged Knee Brace) with an adaptor bracket that transfers load from the subject to the prosthesis. Since the prosthesis remains lateral to the immobilized leg of the healthy subject, the adaptor simulates transfemoral amputee gait without geometric interference from the immobilized leg. While the adapter allows for preliminary testing of the gait control algorithm, the setup does involve certain drawbacks in simulating prosthetic gait, some of which include 1) compliance of the soft tissue interface between the device and user (more so than exhibited by a limb/socket interface), 2) “parasitic” inertia of the intact lower limb (i.e., in addition to the inertia of the prosthesis), and 3) asymmetry in the frontal and axial planes which results in a larger than normal planar moments (i.e., as seen in Fig 10). Despite these, the adaptor provides a reasonable facsimile of amputee gait, and enables testing of the device and proposed impedance-based control approach.

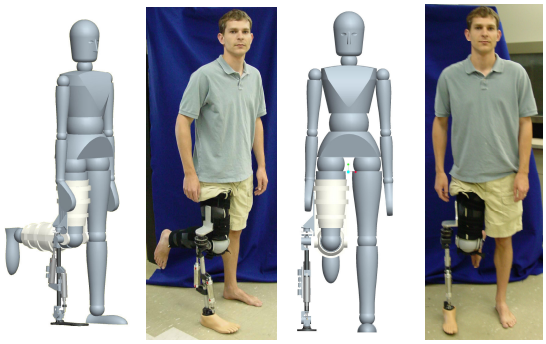

Figure 4-10. Able-bodied testing adaptor for enabling development, testing, and evaluation of the prosthesis and controllers prior transfemoral amputee participation.

The prosthesis was tethered to a 2 MPa (300 psig) pressure source (i.e., compressed nitrogen) and to a controller implemented via a desktop PC with the real-time interface provided by MATLAB Real Time Workshop. Gait trials were performed on a treadmill, which provided a controlled walking speed and

enabled enhanced safety monitoring, including a safety suspension harness and the use of handrails. Unlike the parameter tuning shown in Table 1 and Fig. 9, the gait data for the prosthesis and user did not exist a priori. As such, the parameters shown in Table 1 were used as a starting point, and the parameters were tuned to the user via a combination of joint sensor data, video recordings and user feedback. For example, if the user felt that a joint was not generating necessary torques during support or push off, the stiffness would be increased or the stiffness set point altered. With this iterative process, the impedance functions were tuned, finally resulting in the set indicated in Table 2. Based on this parameter set, the (measured) prosthesis joint angles and torques during level treadmill walking at 0.675 m/s (1.5 mph) are shown in Figures 11 and 12.

Table 4-2. Impedance parameters derived by experimental tuning.

Mode	**Knee Impedance**				**Ankle Impedance**			
	k_1 (N.m/deg))	k_2 (N.m/deg^3)	b (N.m.s)	θ_e (deg)	k_1 (N.m/deg))	k_2 (N.m/deg^3)	b (N.m.s)	θ_e (deg)
1	7.5	0	0	14	4.5	0	0	-8
2	1.0	0.006	0	16	4.5	0	0	-25
3	0	0	0.005	0	0.5	0	0	0
4	0.08	0	0.08	30	0.75	0	0	-3

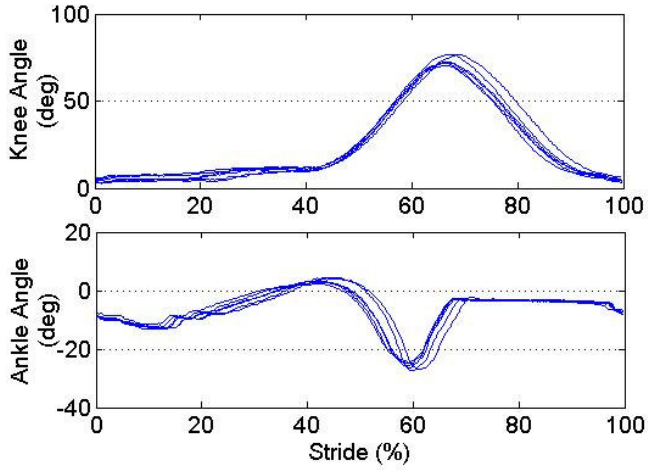

Figure 4-11. Measured joint angles (degrees) for six consecutive gait cycles for a treadmill walk (1.5mph).

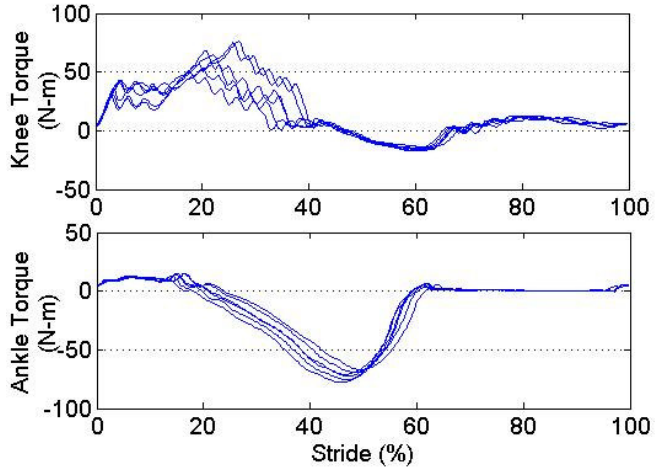

Figure 4-12. Measured joint torques (N.m) for six consecutive gait cycles for a treadmill walk.

In comparing the knee and ankle angles and torques of Figs. 11 and 12 to the prototypical data from Winter (1991) (shown in Figs. 7 and 9), one can observe that the powered prosthesis and controller provide behavior quite similar to normal gait, except in the knee behavior during the first 20% of the stride (i.e., just after heel strike). The difference in behavior during this period is most likely a result of the significant compliance between the adaptor and user. Specifically, the role of the knee during this period is to flex slightly upon impact, which absorbs energy and cushions the impact of heel strike. As such, the knee acts effectively as a stiff spring, first absorbing the energy of impact and shortly after returning this energy to the

user. When used with the adaptor, this knee stiffness acts in series with the (much lower) stiffness of the user/adaptor interface, and thus the cushioning role of knee flexion during heel strike is dominated by the compliance in the user/adaptor interface. This behavior is evident by watching the relative motion between the top of the brace and the subject's hip during heel strike. The authors assume that once the axial compliance between the user and prosthesis is reduced significantly (as would be the case with an amputee subject), the knee joint will exhibit the flexion and subsequent extension evidenced in the prototypical gait kinematics of Fig. 7.

The knee and ankle joint powers, which were computed directly from the torque and differentiated angle data, are shown in Fig. 13, and indicate that the prosthesis is supplying a significant amount of power to the user. Note that the measured power compares favorably to that measured for healthy subjects (see Winter, 1991), and thus indicates an enhanced level of functionality relative to existing passive prostheses.

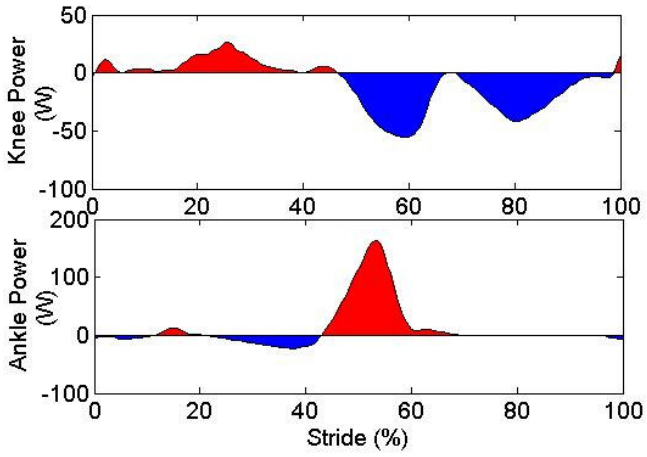

Figure 4-13. Averaged measured joint powers (W) for six consecutive gait cycles for a treadmill walk.

7. Conclusion

This paper described the design and control of a tethered pneumatically actuated transfemoral

prosthesis. The prosthesis design was optimized to provide the requisite joint torque/angle requirements with a minimum volume actuator configuration. The control approach segments the gait cycle into four modes and utilizes a passive impedance characterization of each mode to generate the required torques for the knee and ankle joints during walking. The approach was validated against normal gait data and through experimental testing with an able-bodied adaptor. Test results showed the prosthesis was able to produce a near-normal gait pattern, deliver required joint torques, and supply a significant amount of power to the user.

8. References

Au, S. Bonato, P., Herr, H., "An EMG-Postion Controlled System for an Active Ankle-Foot Prothesis: An Initial Experimental Study," Proceedings of the IEEE Int Conf. on Rehabilitation Robotics, pp. 375-379, 2005.

Clauser CE, McConville JT, Young JM, "Weight, volume and center of mass of segments of the human body. AMRL-TR-69-70, Wright Patterson Airforce Base, Dayton, Ohio, 1969.

DeVita, P., Torry M., Glover, K.L., and Speroni, D.L.,"A Functional Knee Brace Alters Joint Torque and Power Patterns during Walking and Running," Journal of Biomechanics, vol. 29, no. 5, pp. 583-588, 1996.

Donath, M., "Proportional EMG Control for Above-Knee Prosthesis', Department of Mechanical Engineering Masters Thesis, MIT, 1974.

Fite, K.B., and Goldfarb, M. Design and Energetic Characterization of a Proportional-Injector Monopropellant-Powered Actuator, IEEE/ASME Transactions on Mechatronics, vol. 11, no. 2, pp. 196-204, 2006.

Fite, K.B., Mitchell, J., Barth, E.J., and Goldfarb, M. A Unified Force Controller for a Proportional-Injector Direct-Injection Monopropellant-Powered Actuator, ASME Journal of Dynamic Systems, Measurement and Control, vol. 128, no. 1, pp. 159-164, 2006.

Flowers, W.C., "A Man-Interactive Simulator System for Above-Knee Prosthetics Studies, Department of Mechanical Engineering PhD Thesis, MIT, 1973.

Flowers, W.C., and Mann, R.W., “Electrohydraulic knee-torque controller for a prosthesis simulator,” ASME Journal of Biomechanical Engineering, vol. 99, no. 4, pp. 3-8., 1977.

Goldfarb, M., Barth, E.J., Gogola, M.A. and Wehrmeyer, J.A., “Design and Energetic Characterization of a Liquid-Propellant-Powered Actuator for Self-Powered Robots.,” IEEE/ASME Transactions on Mechatronics, vol. 8, no. 2, pp. 254-262, 2003.

Gordon, CC, B. Bradtmiller, T. Churchill, C.E. Clauser, J.T. McConville, I. Tebbetts and R. Walker, “1988 Anthropometric Survey of US Army Personnel: Methods and Summary Statistics,” Technical Report NATICK/TR-89/044, U.S. Army Natick Research, Development and Engineering Center, Natick, MA, 1989.

Grimes, D. L., “An Active Multi-Mode Above Knee Prosthesis Controller. Department of Mechanical Engineering PhD Thesis, MIT., 1979.

Grimes, D. L., Flowers, W. C., and Donath, M., “Feasibility of an active control scheme for above knee prostheses. ASME Journal of Biomechanical Engineering, vol. 99, no. 4, pp. 215-221, 1977.

Hogan, N., Impedance Control: An approach to manipulation: Part 1 - theory, Part 2 - Implementation, and Part 3 - Applications, ASME Journal of Dynamic Systems, Measurement and Control, vol. 107, pp. 1-24, 1985.

Jacobs, R., Bobbert, M.F., van Ingen Schenau, G.J.; “Mechanical output from individual muscles during explosive leg extensions: the role of biarticular muscles,” Journal of Biomechanics, vol. 29, no. 4, pp. 513-523, 1996.

Klute, G.K., Czerniecki, J., Hannaford, B., “Development of Powered Prosthetic Lower Limb, Proceedings of the First National Meeting, Veterans Affairs Rehabilitation Research and Development Service, 1998.

Klute, G.K., Czerniecki, J., Hannaford, B., “Muscle-Like Pneumatic Actuators for Below-Knee Prostheses, Proceedings the Seventh International Conference on New Actuators, pp. 289-292, 2000.

Mochon, S., and McMahon, T.A. Ballistic Walking, Journal of Biomechanics, vol. 13, no. 1, pp. 49-57, 1980.

Nadeau, S., McFadyen, B.J., and Malouin, F., “Frontal and sagittal plane analyses of the stair climbing task in healthy adults aged over 40 years: What are the challenges compared to level walking?,” Clinical Biomechanics, vol. 18, no. 10, pp. 950-959., 2003.

Nagano, A., Ishige, Y., and Fukashiro, S., “Comparison of new approaches to estimate mechanical output of individual joints in vertical jumps,” Journal of Biomechanics, vol. 31, no. 10, pp. 951-955, 1998.

Popovic, D. and Schwirtlich, L., “Belgrade active A/K prosthesis, “ in de Vries, J. (Ed.), Electrophysiological Kinesiology, Interm. Congress Ser. No. 804, Excerpta Medica, Amsterdam, The Netherlands, pp.

337–343, 1988.

Popovic D, Oguztoreli MN, Stein RB., “Optimal control for an above-knee prosthesis with two degrees of freedom,” Journal of Biomechanics, vol. 28, no. 1, pp. 89-98, 1995.

Prilutsky, B.I., Petrova, L.N., and Raitsin, L.M., “Comparison of mechanical energy expenditure of joint moments and muscle forces during human locomotion,” Journal of Biomechanics, vol. 29, no. 4, pp. 405-415, 1996.

Riener, R., Rabuffetti, M., and Frigo, C., “Joint powers in stair climbing at different slopes.”, Proceedings of the IEEE International Conference on Engineering in Medicine and Biology, vol. 1, p. 530., 1999.

Shields, B.L., Fite, K., and Goldfarb, M. Design, Control, and Energetic Characterization of a Solenoid Injected Monopropellant Powered Actuator, IEEE/ASME Transactions on Mechatronics, vol. 11, no. 4, pp. 477-487, 2006.

Stein, J.L., “Design Issues in the Stance Phase Control of Above-Knee Prostheses,” Department of Mechanical Engineering PhD Thesis, MIT, 1983.

Stein, J.L., and Flowers, W.C., “Stance phase control of above-knee prostheses: knee control versus SACH foot design,” Journal of Biomechanics, vol. 20, no. 1, pp. 19-28, 1988.

Waters, R., Perry, J., Antonelli, D., and Hislop, H., “Energy cost of walking amputees: the influence of level of amputation,” J. Bone and Joint Surgery. 58A, 42–46, 1976.

Winter, D. A. and Sienko, S. E., “Biomechanics of below-knee amputee gait,” J. Biomechanics. 21, 361–367., 1988.

Winter, D.A., “The biomechanics and motor control of human gait: normal, elderly and pathological,” University of Waterloo Press, 2nd ed. , 1991.

CHAPTER V

ADDENDUM TO MANUSCRIPT II

1. Experimental Testing Setup

In order to validate the integrity of the leg and control systems, a two-fold laboratory setup was implemented. First, to test the structural integrity of the prosthesis and to tune the torque controller a fixed mount was employed as in Figure 5-1.

Figure 5-1. Picture of fixed mount setup.

The second part of the testing was completed using the able-bodied adaptor before actual subject

testing on amputees. In order to provide a controlled environment for assessment and tuning of the device, a treadmill was employed along with safety devices (i.e. support harness and handrails). The overall setup is presented in Figure 5-2.

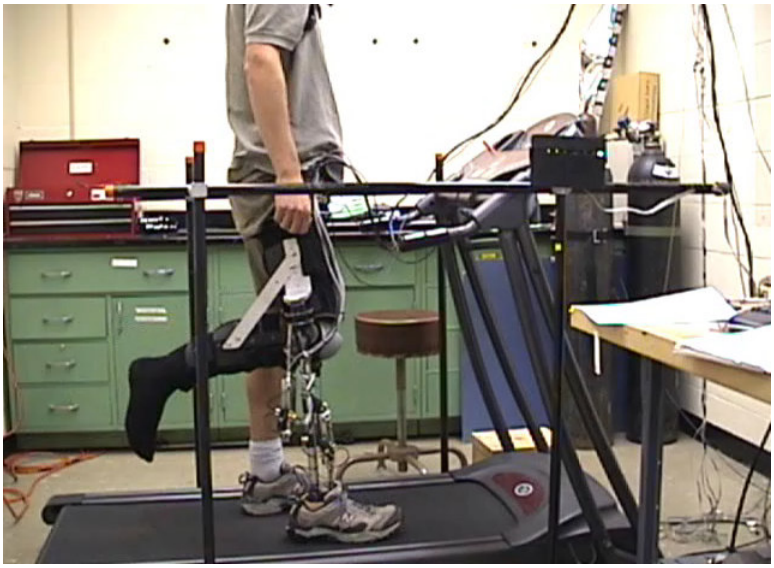

Figure 5-2. Picture of treadmill testing setup.

2. Electronics boards

2.1 On-board Analog Circuit Board

The transfemoral prosthesis was designed to house a small onboard analog electronics board measuring (0.78” x 5.20”) within the shank tubing. The purpose of the board is to provide a central bus for power and ground, signal routing, buffering and amplification for all onboard sensors. All signals and power are routed to and from the board through a 50 ft. round jacket flat cable tether (3M model 3759/26) with wire layout in Appendix C-1. The central bus functionality distributes +15 and –15 volts and ground to the board. On the board two voltage regulating diodes are used to supply +10 and +5V to the sensors. To mitigate noise issues in small signal output from load cells the board amplifies the signals from the ankle

and knee torque load cells and for each of the three axes of the socket load cell. Finally, the board buffers the output of the knee and ankle potentiometers. The complete schematic and accompanying layout and trace diagrams for the onboard analog circuit are presented in Appendix C-2. The final board was designed with ExpressPCB software and manufactured by ExpressPCB.

2.2 Off-board Analog Circuit Board

The functionality of the off-board circuit board is two-fold. The first use is to route the signals between the prosthesis via the tether to the computer. For the prosthesis it provides filtering for the ankle and knee torque sensors, analog differentiation of the position signals, and a servo amplifier. The servo amplifier is design to proportionally output ±1 amp from an input signal ranging from ±10V. The second function of the board is to route signals from a sound leg sensor package consisting of foot switches, potentiometers and a gyroscope. The schematics and layout for the off board circuit are presented in Appendix C-3.

3. Control and Tuning

The control of the prosthesis involves controlling the position and torques at the knee and ankle joints and involves two nested loops. The inner loop is a PID torque controller and the outer loop outputs a desired torque generated by the impedance based control approach outlined in Chapter IV and further explained in Bohara (2006). The approach was implemented using Matlab Simulink and Real-Time Workshop and the models for the knee and ankle joint control can be found in Appendix D.

Once the control loops were implemented the gains appropriate gains were determined experimentally by starting with the torque control gains. With the prosthesis in a fixed mount setup and with the motion of

the prosthesis constrained physically by a person, the torque controller was tuned with sine wave torque input with maximum amplitude of 30 Nm and frequency of 1.0 Hz. The resulting gains of the tuning are presented in Table 5-1 and the tracking data in Figures 5-3 and 5-4. As an additional test of the torque tracking capabilities of the device the stiffness tracking of knee and ankle joints is presented in Figures 5-5 and 5-6. The data was obtained experimental using the impedance based controller by Bohara (2006) by a user walking with the able bodied adaptor. As demonstrated in the plots and degree of alignment is present between the actual and desired stiffnesses, proving the capability of the device to generate the desired torques. It should be noted in Figure 5-5 that the ankle is capable of producing the 100 Nm of torque dictated by biomechanical data.

Table 5-1. PID control gains for force control loop.

Mode	Ankle Joint	Knee Joint
Proportional	0.01	0.01
Integral	0	0
Derivative	0	0

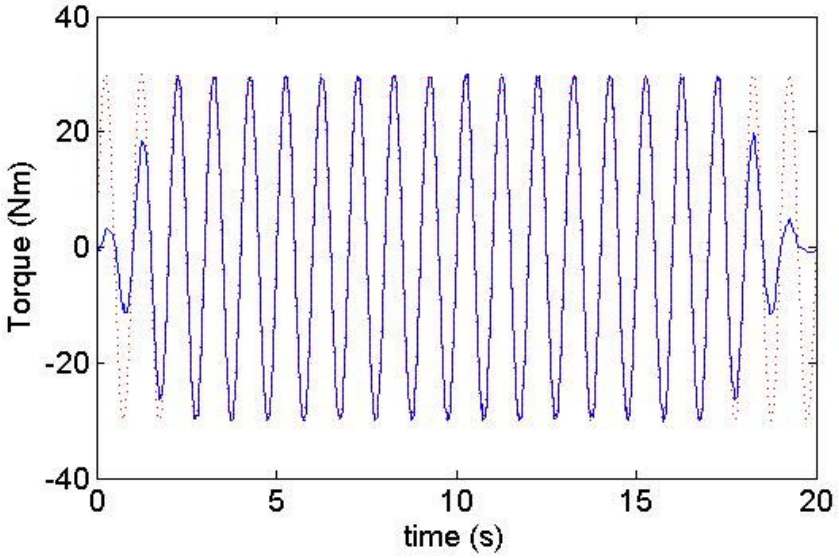

Figure 5-3. Knee actuator torque tracking to 1.0 Hz sine wave with a 30 Nm amplitude. The dotted line represents the desired and the solid line is the actual.

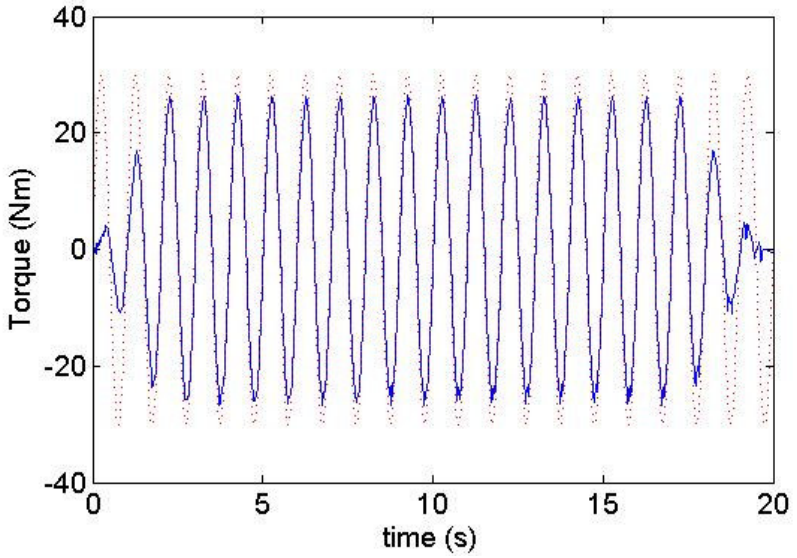

Figure 5-4. Ankle actuator torque tracking to 1.0 Hz sine wave with a 30 Nm amplitude. The dotted line represents the desired and the solid line is the actual.

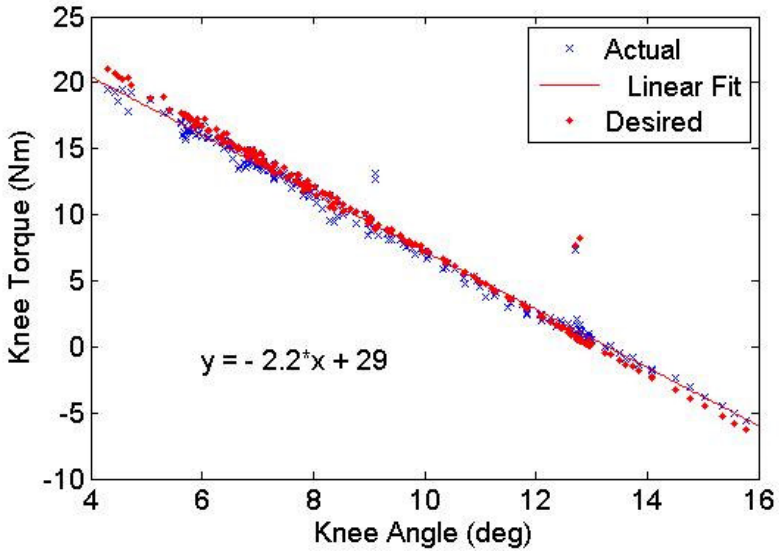

Figure 5-5. Knee stiffness during walking experiments desired knee stiffness of 2 Nm/deg and actual is 2.2 Nm/deg.

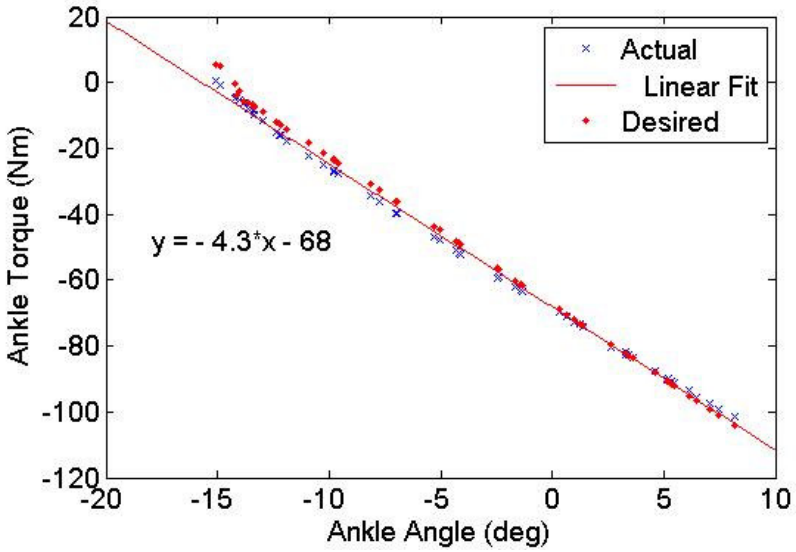

Figure 5-6. Ankle stiffness in walking experiments desired ankle stiffness of 4.5 Nm/deg and actual is 4.3 Nm/deg.

4. Design Review

This thesis represents the first approach at a powered knee and ankle transfemoral prosthesis. The initial qualitative assessment of the leg in conjugation with the data presented in this thesis is that the prosthesis is capable of performing the required tasks of a powered lower limb prosthesis. Throughout the initial assessment of the prototype notes were made regarding functionalities of the leg and are presented in Table 5-2.

Table 5-2. Design Improvement Summary

Functionality/ Component	Comment	Recommendation

Functionality/ Component	Comment	Recommendation
Servovalves	Several attempts were made to upgrade the current commercial servovalves used on the device to custom spool and sleeve valves as depicted in Manuscript I. However limitations in encoder resolution, gearhead backlash, and torque limitations in iterative devices lead to successful implementation.	Implement custom spool and sleeve servovalves on the device to improve response and mass flow through servovalves. A successful implementation of valves requires using a spool and sleeve combination with a large flow coefficient and motor capable of driving it and a zeroing mechanism that is reliable and repeatable.
Dry Bearings	The knee joint shaft is slightly undersized and allows for a wobble in the joint in the sagittal plane and maybe a possible source of instability in knee joint actuation.	Ensure components machined to bearing manufacturers specifications.
Shank	The prototype design was modeled after traditional prosthesis fitting methods were the shank section is cut to size a specific user. However, for prototype design this may lead to excess time in manufacturing custom legs for each test subject and add time delays and expense to overall project.	Design a shank section that allows for adjustability once assembled.
Hard Stops of Joints	The design of the joints requires hard stops to restrict the motion of the joint to the desired range. The hard stops were designed to be hard rubber, but under the severe loading and pressure even the hardest rubber of duromter Shore 90A.	Decrease spacing of rubber hard stops from 1/8” and replace with thin rubber sheeting capable of the resisting the loads.
Able-Bodied Adaptor	The adaptors functionality could be enhanced if it was stiffened all 3 moment planes and in axial load direction to better mimic true prosthesis user interaction.	Develop a more secure and stable platform to attach prosthesis to able-bodied subject.

Functionality/ Component	Comment	Recommendation
3-Axis Socket Load Cell	The socket load cell design as-is is prone slippage due to axial torques.	Physical mating and asymmetry of pieces of the cross, load transmitter and pyramid adaptor could assist and resisting the load.

5. References

Bohara, Amit, “Finite State Impedance Based Control of Powered Transfemoral Prosthesis” Department of Mechanical Engineering Masters Thesis, Vanderbilt University, 2006.

APPENDIX A

PARTS LISTS

Table A-1. Prosthesis Prototype Components

Part No.	Name	Description	File Name
1	Leg Assembly	Main Leg Assembly file	LEG-V2.asm
2	Shank Joint Tube	Main support for leg. Connects joint to tube.	TUBE_LEG.prt
3	Connector		JOINT_TUBE_CONNECTER.prt
4	Joint Angle Bracket	Cantilever joint support.	JOINT_ANGLE_BRACKET.prt
5	Joint Axle and Pot Housing	Integrated pot housing in joint axle.	JOINT_AXLE_POT_HOUSING.prt
6	Garlock Dry Bearings	Garlock BB2017DU Bearing	GARLOCK_BEARING_BB2017DU.prt
7	Snap Ring	¾" Snap ring, holds outer joint race on to joint axle.	SNAP_RING_3_4.prt
8	Potentiometers	ETI Systems – SP12S – 10K	HONEYWELL_POT_.prt
9	Ankle Joint Outer Race	N/a	CANTILEVER_KNEE_OUTER_RACE.prt
10	Knee Joint Mount	Connector between knee outer race and socket load cell.	CANTILEVER_KNEE_JOINT_MOUNT.prt
11	Joint Race End Cap	End cap attaches to outer joint race and attachment point for potentiometer.	CANTILEVER_JOINT_RACE_ENDCAP.prt
12	Rubber Bumper	95 Shore A rubber to provide mechanical stop for joint rotation.	BUMPER.prt

Part No.	Name	Description	File Name
13	Ankle Joint Outer Race	N/a	CANTILEVER_ANKJOINT_OUT_RACE.prt
14	Female Pyramid Slider	Standard Female slider connector integrated into ankle joint	FEMALE_PRYIMADSLIDER.prt
15	Ankle Clamp	Attaches ankle cylinder to shank	ANKLE__CLAMP.prt
16	Knee Clamp	Attaches knee cylinder to shank	KNEE_CLAMP2PRT.prt
17	Clamp Pin	Pivot pin between cylinder and clamp	CLAMP__PIN.prt
18	Clevis Pin	Pivot pin between cylinder and clevis	CLEVIS_PIN.prt
19	Ankle Cylinder	Bimba 1.5” Cylinder part: 17-2.75-DP	15_275_PISTONCYLINDAR.prt
20	Knee Cylinder	Bimba 1.5” Cylinder part: 17-3-DP	15_3_PISTONCYLINDAR.prt
21	Load Cell	Honeywell Sensotec Model 31	ELPS-T3.prt
22	Clevis	Ankle Clevis – Bimba Part no: D-166-3	ROD_CLEVIS_25.prt
23	Clevis	Knee Clevis - Custom	ROD_CLEVIS_25_LONG.prt
24	Lo Rider Foot w/ cosmesis covering	Otto Bock Lo Rider Foot sizes (25, 28)	FLEX_FOOT_AXIA_.prt

Table A-2. Socket Load Cell Components

Part No.	Name	Description	File Name
1	Socket Load Cell	Assembly file	MALCROSS_CIRLC.asm
1	Cross Pattern Disc	N/a	MALCROSS_CIR
2	Load Transmitter	N/a	MC_ROD
3	Housing	N/a	MALCROSS_HOUSE
4	Base	N/a	MALCROSS_CIRCLE_MOUNT.prt
5	Spacer	N/a	MC_TOPMOUNT.prt
6	Pyramid Connector	Standard pyramid connector milled to specs.	PYRAMID_DISK_.prt

Part No.	Name	Description	File Name
7	Strain Gages Part no. EA-06-125AC-350	Vishay Micromeasurements Linear Pattern Gage	n/a

Table A-3. Able-Bodied Adaptor Components

Part No.	Name	Description	File Name
1	Knee Immobilizer Part No. WM-94001	KneeRanger – Universal Hinged Knee Brace, Large	n/a
2	Female Pyramid Connector	Standard 4-hole bolt pattern connector	n/a
3	Angle Mount	Custom-made to fit, no drawings.	n/a

APPENDIX B

OPTIMIZATION CODES

6. Kinematic Configuration

6.1 Ankle Kinematic Configuration Optimization

```
% Frank Sup
% Vanderbilt University
%Find Ankle Dimensions
% m-file to find min actuator volume for Bimba pneumatic actuators

%Declare Variables
N=100;
l1_v=linspace(.001,.10,N); %m
%L_v=linspace(.05,.2,N); %m
theta_v=linspace(25,115,N); %degrees
%D_v=linspace(.01,.05,N); %m
D_v=[7/8,17/16,1.25,1.5,1.75,2 %
        ;3.56,3.84,4.72,4.38,5.75,5.62].*.0254; %Enter inches converts to meters
str_v=linspace(.25,12,48).*.0254; %enter inches, converts to m
clevis_v=[1.49,1.49,1.49,1.49,1.49,1.49]*.0254; %with Load Cell .59 enter inches, converts to m
Ps=300*4.45*39.3^2; %pascals
Td=130; %Nm
deltathetad_v=linspace(65,75,N).*pi./180; %radians
l2_max=.3; %m
Vmin = (D_v(2,6)+.001)*D_v(1,6)^2*pi*.25; %m^3
l1_final=100; %m
l2_final=0; %m
L_final=D_v(2,6); %m
str_final=str_v(12); %m
D_final=D_v(1,6); %m
T_final=1000; %Nm
theta1_final=0; %radians
```

```
theta2_final=0; %radians
deltatheta_final=0; %radians
theta_hat_final=0; %radians
thetadiffd=pi; %radians
thetashift=10*pi/180; %radians
Tmax=0; %Nm

for hh=1:N,
    deltathetad=deltathetad_v(hh);
for ii=1:N,
    l1=l1_v(ii);
    for jj=1:6,
        L=D_v(2,jj);
        clevis=clevis_v(jj);
            for kk=1:48,
                str=str_v(kk);
                for ll=1:N,
                    theta=theta_v(kk)*pi/180;
                    L1=L+str+clevis;
                    L2=L+2*str+clevis;

                    %Calculate l2 for desired range of motion
                    l21=sqrt(l1^2+L1^2-2*l1*L1*cos(pi-asin(l1*sin(theta)/L1)-theta));

l22=sqrt(l1^2+L2^2-2*l1*L2*cos(pi-asin(l1*sin(theta+deltathetad)/L2)-(theta+deltathetad)));

                    %Check if l21 and l22 are within desired tolerance
                    if abs(l22-l21)>(l1_v(1)/10)
                        break
                    end

                    %Average l2 calcuations
                    l2=(l21+l22)/2;

                    %Break if calculated l2 is greater then tolerances
                    if l2>l2_max,
                        break
                    end

                    %Calculate values for theta1 and theta2
                    theta1=acos((l1^2+l2^2-(L1)^2)/(2*l1*l2));
```

```
theta2=acos((l1^2+l2^2-(L2)^2)/(2*l1*l2));

%Remove any imaginary results
if imag(theta1)~=0 | imag(theta2)~=0
    break
end

%Calculate delta theta
deltatheta=theta2-theta1;

%Confirm Delta theta has acceptable range of motion
if deltatheta<70*pi/180,
    break
end

% combination provides desired range of motion, now find if
% combination provides desired torque within range of motion
theta_hat=acos(.5*((l1/l2)+(l2/l1)-sqrt(((l1/l2)+(l2/l1))^2-4)));
if (theta_hat < theta1)|(theta_hat > theta2),
    break
end

% maximum torque occurs within range of motion


    D=D_v(1,jj);
    A=D^2*pi*.25;

    %Find torque at required shift for max torque

T=Ps*A*(l1*l2*sin(theta1+thetashift)/sqrt(l1^2+l2^2-2*l1*l2*cos(theta1+thetashift)));

    %Volume Calculation
    V=L1*A;

    %Shift from theta1 to theta_hat to match actual knee data
    %for shift.
    thetadiff=abs(theta1-theta_hat+thetashift);

    %If Volume is less then Vmin and has desired or greater
    %torque store values.
```

```
                        if V <= Vmin & T >= Td & l1 <= l1_final,
                            thetadiffd=thetadiff;
                            Vmin=V;
                            l1_final=l1;
                            l2_final=l2;
                            L_final=L;
                            str_final=str;
                            D_final=D;
                            T_final=T;
                            theta1_final=theta1;
                            theta2_final=theta2;
                            deltatheta_final=deltatheta;
                            theta_hat_final=theta_hat;

Tmax=Ps*A*(l1*l2*sin(theta_hat_final)/sqrt(l1^2+l2^2-2*l1*l2*cos(theta_hat_final)));
                        end
                    end %ll=1:N
                end %kk=1:12
            end %jj=1:12
end %ii=1:N
end %hh=1:N

%Print out results.
Vmin
l1_final
l2_final
L_final=L_final/.0254
str_final=str_final/.0254
D_final=D_final/.0254
T_final
Tmax
theta1_final=theta1_final*180/pi
theta2_final=theta2_final*180/pi
deltatheta_final=deltatheta_final*180/pi
theta_hat_final=theta_hat_final*180/pi
thetadiffd=thetadiffd*180/pi
```

6.2 Knee Kinematic Configuration Optimization

```
% Frank Sup
% Vanderbilt University
```

```
% Find Knee Dimensions
% m-file to find min actuator volume for Bimba pneumatic actuators

N=100;
l1_v=linspace(.04,.10,N); %m
%L_v=linspace(.05,.2,N); %m
theta_v=linspace(10,70,N); %degrees
%D_v=linspace(.01,.05,N); %m
D_v=[7/8,17/16,1.25,1.5,1.75,2 %
            ;3.56,3.84,4.72,4.38,5.75,5.62].*.0254; %Enter inches converts to meters
str_v=linspace(.25,12,48).*.0254; %enter inches, converts to m
clevis_v=[2.3,2.3,2.3,2.3,2.3,2.3]*.0254; %enter inches 1.31=clevis, .59=LoadCell, converts to m
Ps=300*4.45*39.3^2; %pascals
Td=86; %Nm
deltathetad_v=linspace(110*pi/180,140*pi/180,N); %radians
l2_max=.3; %m
Vmin = 1; %m^3
l1_final=100; %m
l2_final=100; %m
L_final=D_v(2,6); %m
str_final=str_v(12); %m
D_final=D_v(1,6); %m
T_final=1000; %Nm
theta1_final=0; %radians
theta2_final=0; %radians
deltatheta_final=0; %radians
theta_hat_final=0; %radians
thetadiffd=pi; %radians
thetashift=35*pi/180; %radians actual at 25 + 10 for bumpers
Tmax=0; %Nm
z=1;

for hh=1:N;
    deltathetad=deltathetad_v(hh);
for ii=1:N,
    l1=l1_v(ii);
    for jj=1:6,
        L=D_v(2,jj);
        D=D_v(1,jj);
        clevis=clevis_v(jj);
            for kk=1:48,
```

```
str=str_v(kk);
for ll=1:N,
    theta=theta_v(kk)*pi/180;
    L1=L+str+clevis;
    L2=L+2*str+clevis;

    %Calculate l2 for desired range of motion
    l21=sqrt(l1^2+L1^2-2*l1*L1*cos(pi-asin(l1*sin(theta)/L1)-theta));

l22=sqrt(l1^2+L2^2-2*l1*L2*cos(pi-asin(l1*sin(theta+deltathetad)/L2)-(theta+deltathetad)));

    %Check if l21 and l22 are within desired tolerance
    if abs(l22-l21)>(l1_v(1)/40)
        break
    end

    %Average l2 calcuations
    l2=(l21+l22)/2;

    %Break if calculated l2 is greater then tolerances
    if l2>l2_max,
        break
    end

    %Calculate values for theta1 and theta2
    theta1=acos((l1^2+l2^2-(L1)^2)/(2*l1*l2));
    theta2=acos((l1^2+l2^2-(L2)^2)/(2*l1*l2));

    %Remove any imaginary results
    if imag(theta1)~=0 | imag(theta2)~=0
        break
    end

    %Calculate delta theta
    deltatheta=theta2-theta1;

    %Confirm Delta theta has acceptable range of motion
    if deltatheta<(115*pi/180),
        break
    end
```

```
% combination provides desired range of motion, now find if
% combination provides desired torque within range of motion
theta_hat=acos(.5*((l1/l2)+(l2/l1)-sqrt(((l1/l2)+(l2/l1))^2-4)));
if (theta_hat < theta1)|(theta_hat > theta2),
    break
end

% maximum torque occurs within range of motion

    A=D^2*pi*.25;

    %Find torque at required shift for max torque
    T=Ps*A*(l1*l2*sin(theta2-thetashift)/sqrt(l1^2+l2^2-2*l1*l2*cos(theta2-thetashift)));

    %Volume Calculation
    V=L1*A;

    %Shift from theta1 to theta_hat to match actual knee data
    %for shift.
    thetadiff=abs(theta2-theta_hat-25*pi/180);

    %If Volume is less then Vmin and has desired or greater
    %torque store values.
    if V <= Vmin & T >= Td,
        S_v(1,z)=l1;
        S_v(2,z)=l2;
        S_v(3,z)=T;
        thetadiffd=thetadiff;
        Vmin=V;
        l1_final=l1;
        l2_final=l2;
        L_final=L;
        str_final=str;
        D_final=D;
        T_final=T;
        theta1_final=theta1;
        theta2_final=theta2;
        deltatheta_final=deltatheta;
        theta_hat_final=theta_hat;

Tmax=Ps*A*(l1_final*l2_final*sin(theta_hat_final)/sqrt(l1_final^2+l2_final^2-2*l1_final*l2_final*cos(theta_h
```

```
at_final)));
                                z=z+1;
                                end
                            end %ll=1:N
                        end %kk=1:12
                    end %jj=1:12
end %ii=1:N
end %hh=1:N;

%Print out results.
Vmin
l1_final
l2_final
L_final=L_final/.0254
str_final=str_final/.0254
D_final=D_final/.0254
T_final
Tmax
theta1_final=theta1_final*180/pi
theta2_final=theta2_final*180/pi
deltatheta_final=deltatheta_final*180/pi
theta_hat_final=theta_hat_final*180/pi
thetadiffd=thetadiffd*180/pi
```

7. Socket Load Cell Volume Minimization

```
% Frank Sup
% Vanderbilt University
% Minimize Socket Load Cell Volume

%Declare Variables
J = 20; %Interval
M = 100; %Nm Max Moment
F = 1000; %N Max Force
E_v = [193e9 70e9]; %Modulus Pa
b_v = linspace(.01,.02,J); %beam width %m
h_v = linspace(.0025,.005,J); %beam thickness %m
t_v = linspace(.01,.022,J); %beam seperation %m
L_v = linspace(.02,.022,J); %beam Length %m
k = 1;
```

```
%Determine configurations that meet meet strain criteria and ratio of bending strain to axial %force strain.
for N = 1:2,
    E = E_v(N);
    for O = 1:J,
        b = b_v(O);
        for P = 1:J,
            h = h_v(P);
            for Q = 1:J,
                t = t_v(Q);
                for R = 1:J,
                    L = L_v(R);

em = M/(t*b*h*E); %microstrain
ef = 3*F*L/(8*E*b*h^2); %microstrain
ratio = ef/em;

if abs(ratio-1)<.4 && em+ef < 1500e-6, %in microstrain
sol(k,1) = b; %beam width
sol(k,2) = h; %beam height
sol(k,3) = t; %beam seperation
sol(k,4) = E; %Modulus
sol(k,5) = em; %strain from Moment
sol(k,6) = ef; %strain from Force
sol(k,7) = L; %beam Lentgh
sol(k,8) = ratio; %ef/em
k = k+1;
end
            end
        end
    end
    end
end
%Review Solution Combinations that minimize volume and return the top 5 smallest %configurations.

tester=1000;
test = ones(5,8);
for N=1:size(sol(:,6)),
    if sol(N,1)*sol(N,3)*sol(N,7)<tester,
    %if abs(sol(N,5)+sol(N,6)-1000e-6) < abs(test(1,6)+test(1,5)-1000e-6),
        test(5,:) = test(4,:);
```

```
        test(4,:) = test(3,:);
        test(3,:) = test(2,:);
        test(2,:) = test(1,:);
        test(1,:) = sol(N,:);
        tester= sol(N,1)*sol(N,3)*sol(N,7);

    end
end
```

APPENDIX C

SCHEMATICS OF ANALOG CIRCUITS

8. On-board Analog Circuit

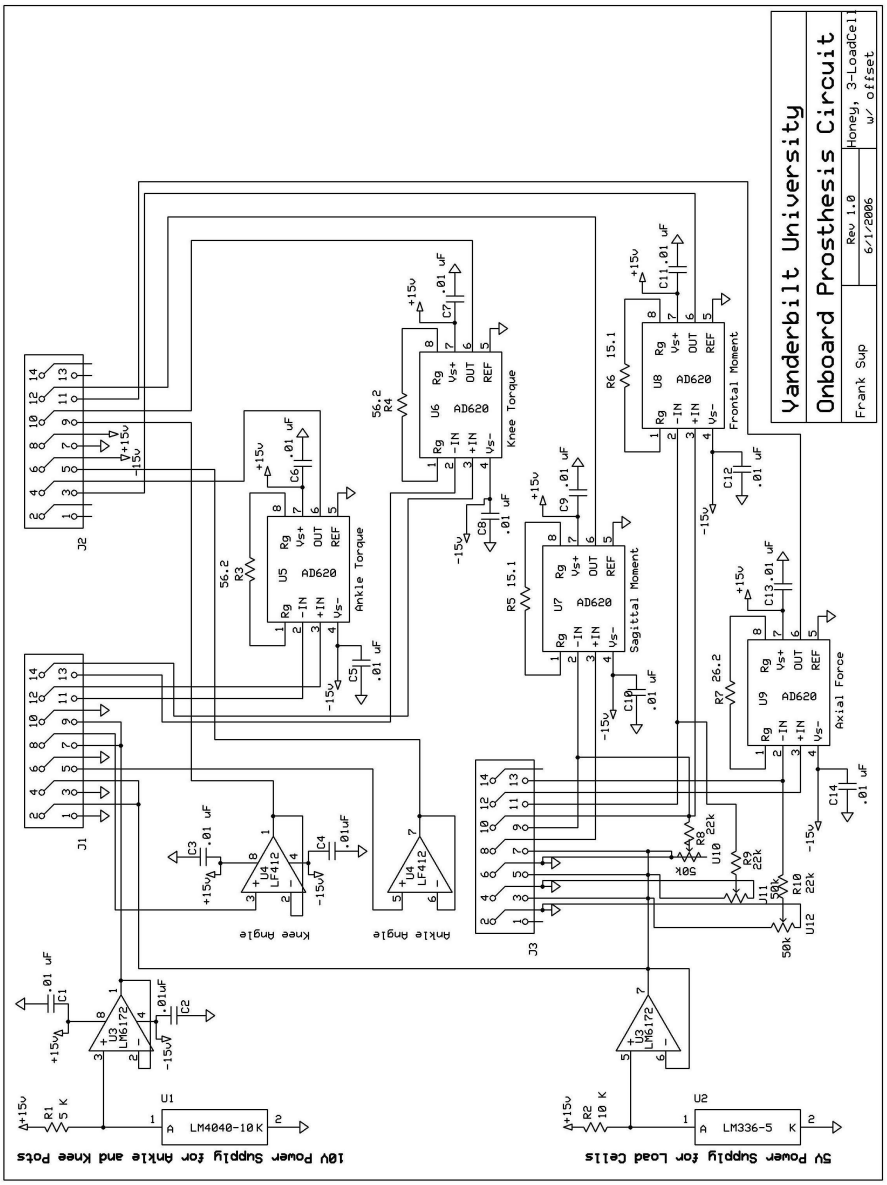

Figure C-1. Schematic of circuit used for onboard sensor power and amplifying.

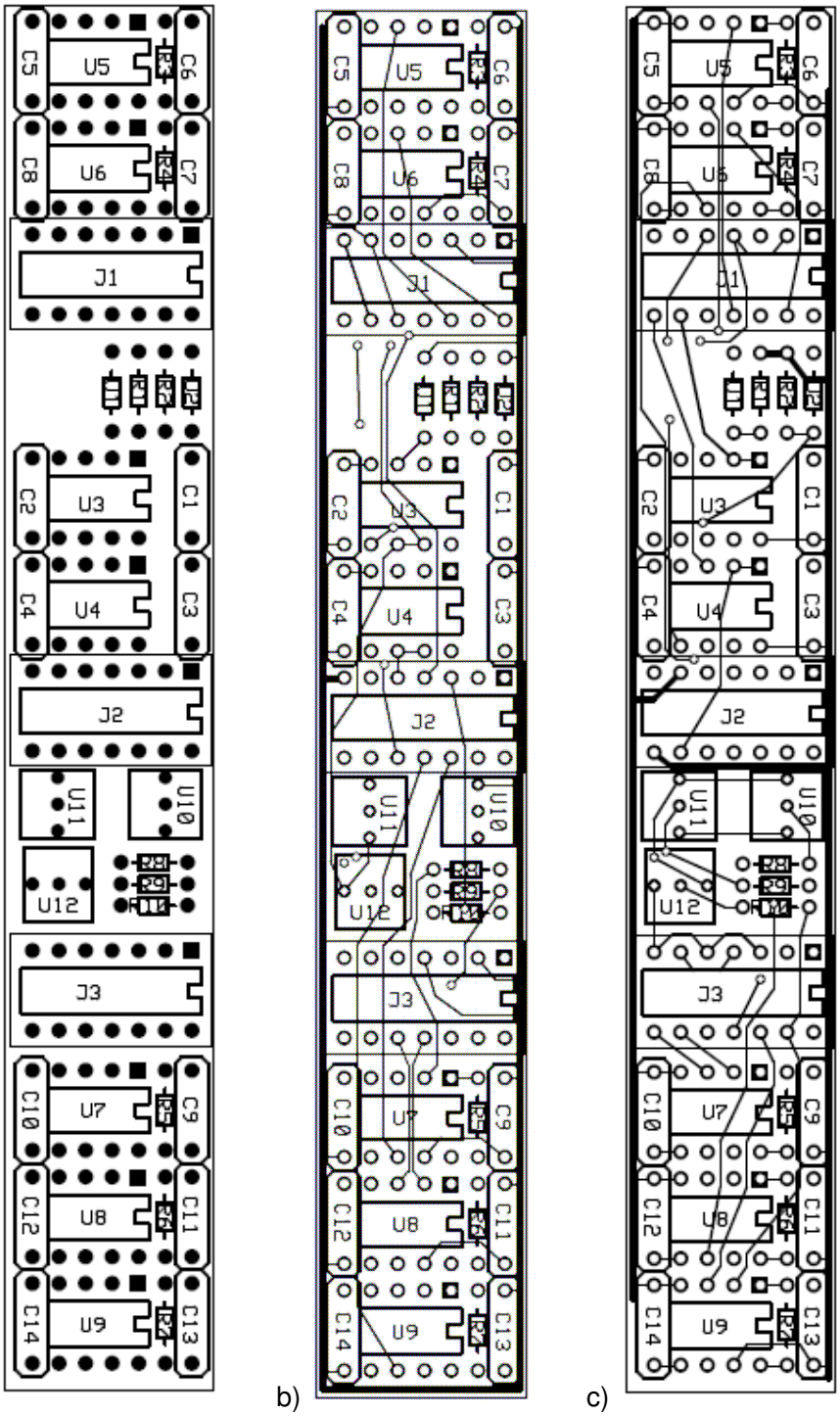

Figure C-2. Board Layout (a), top trace (b) and bottom trace (c) of the circuit used for onboard signal routing and amplification overall dimensions 0.78” x 5.20”. Printed via ExpressPCB software and service.

9. Off board Analog Circuit

Note: The off board analog circuit has been divided into the following three functional schematics in Figures C-3 to C-5 and the all three combined into a common board layout in Figure C-6.

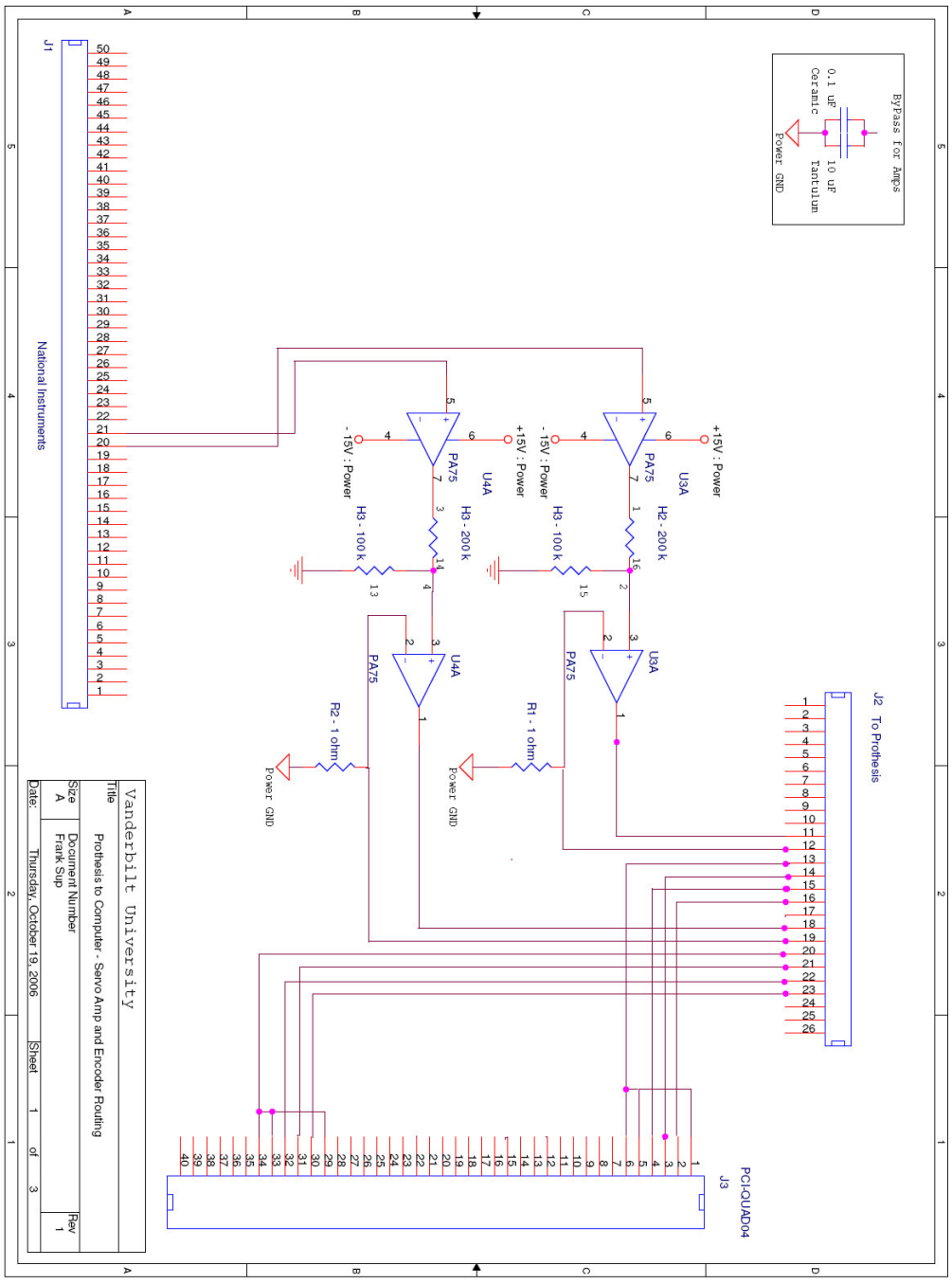

Figure C-3. Schematic of circuit used for off board servo amplifier encoder signal routing.

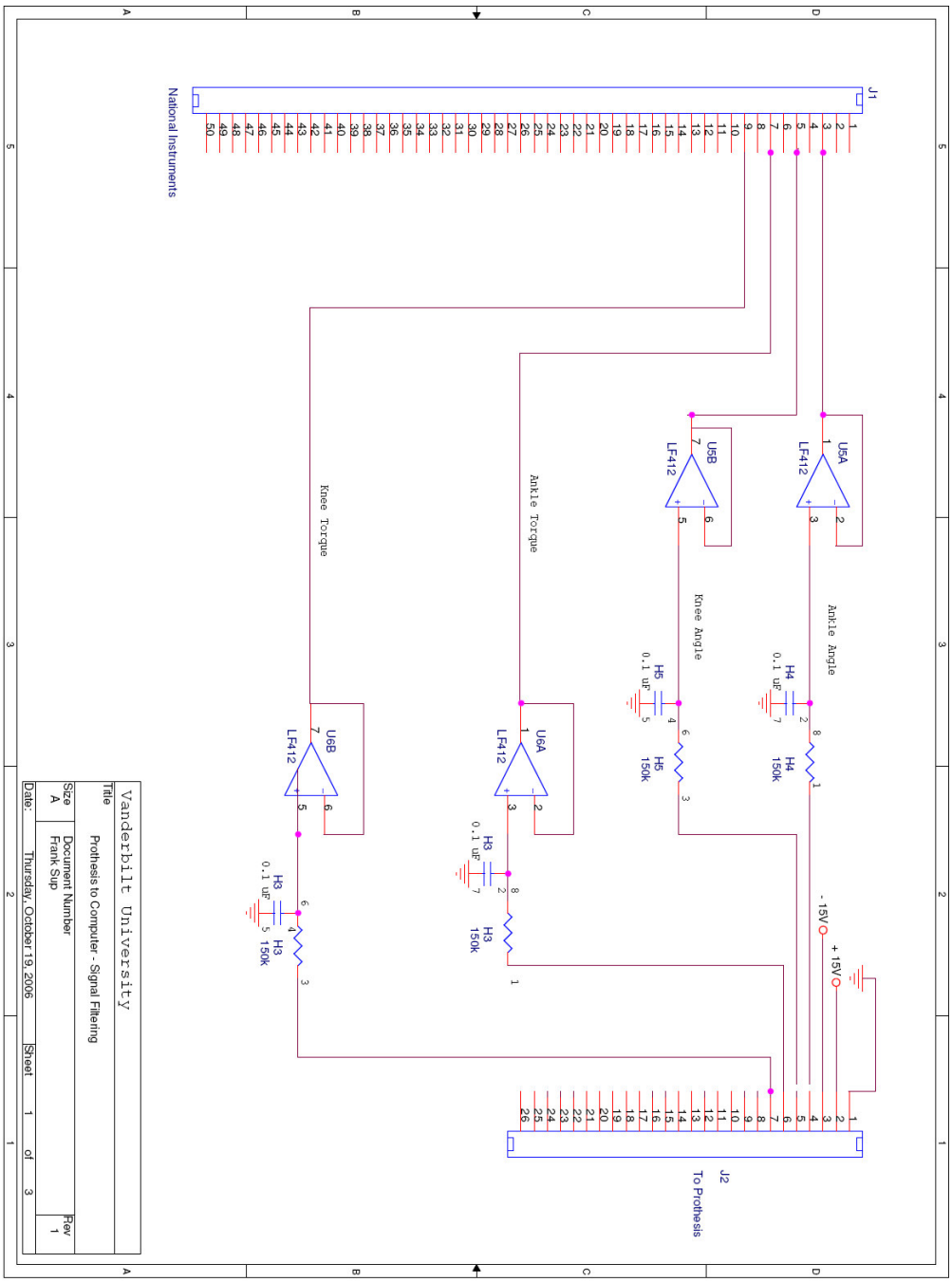

Figure C-4. Schematic of circuit used for off board load cell sensor signal filtering and routing.

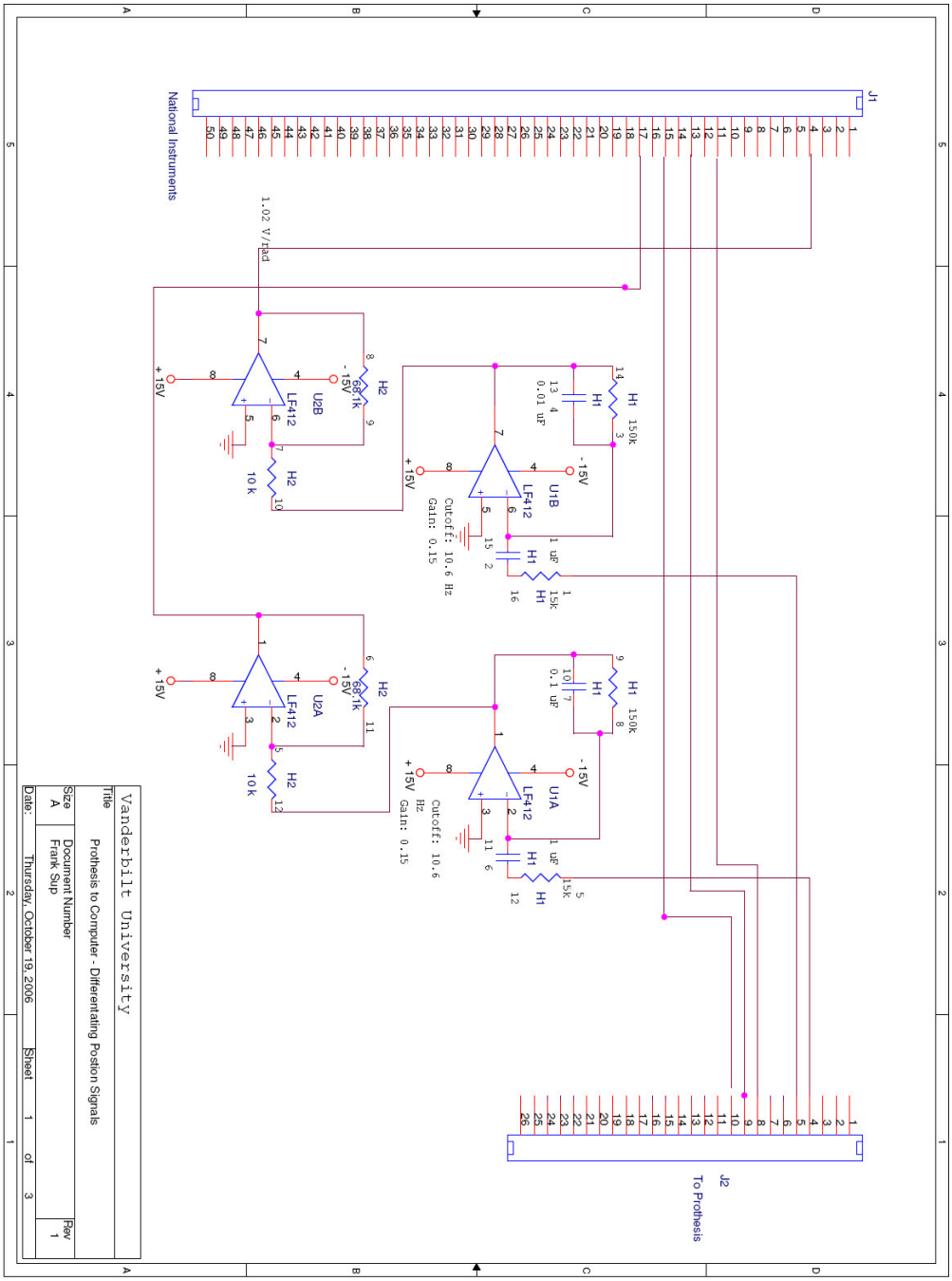

Figure C-5. Schematic of circuit used for off board position sensor signal routing and differentiation.

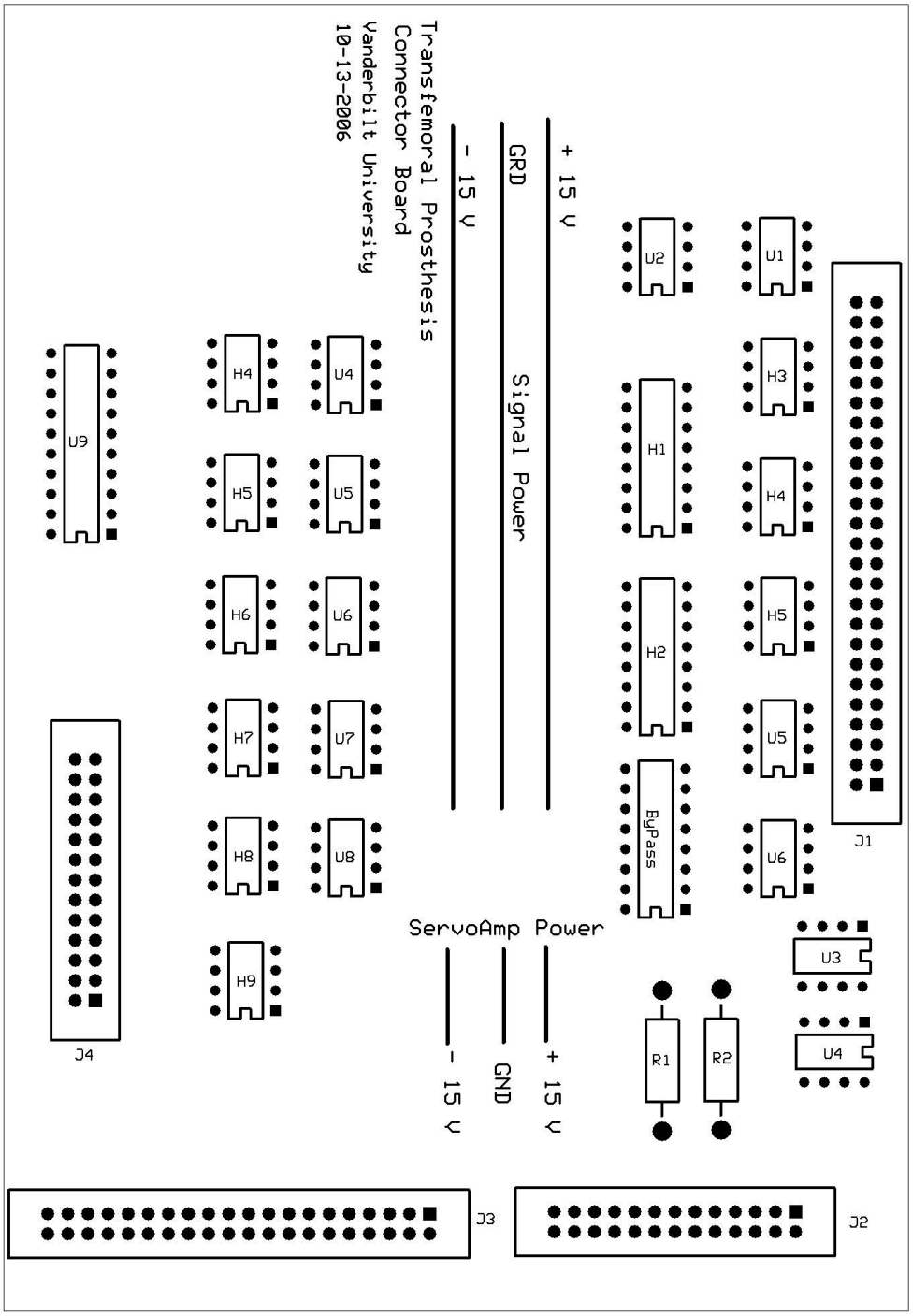

Figure C-6. Board Layout of circuit used for offboard signal processing and for computer input for National Instruments Card PCI-6031E for analog signal routing and Measurement Computing PCI-QUAD04 for encoder signal routing.

APPENDIX D

MATLAB SIMULINK BLOCKS

10. Torque Control

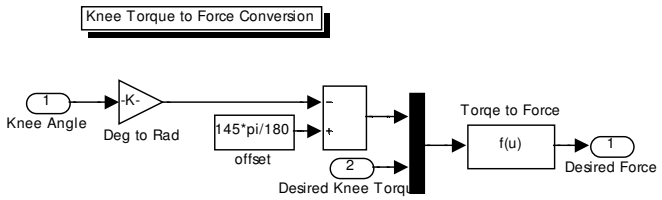

Figure D-1. Knee Torque to Force Conversion subblock for torque control diagram for Matlab Simulink.

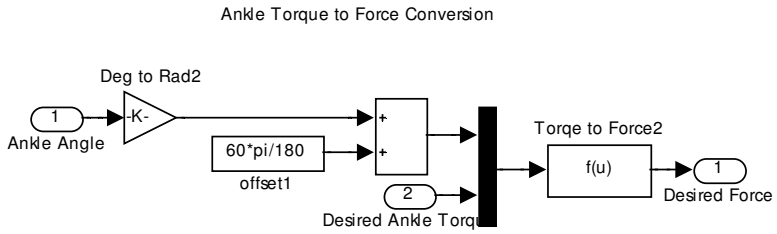

Figure D-2. Ankle Torque to Force Conversion subblock for torque control diagram for Matlab Simulink.

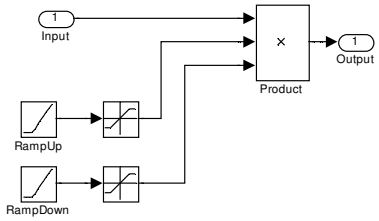

Figure D-3. Ramp up/down subblock for torque control diagram for Matlab Simulink.

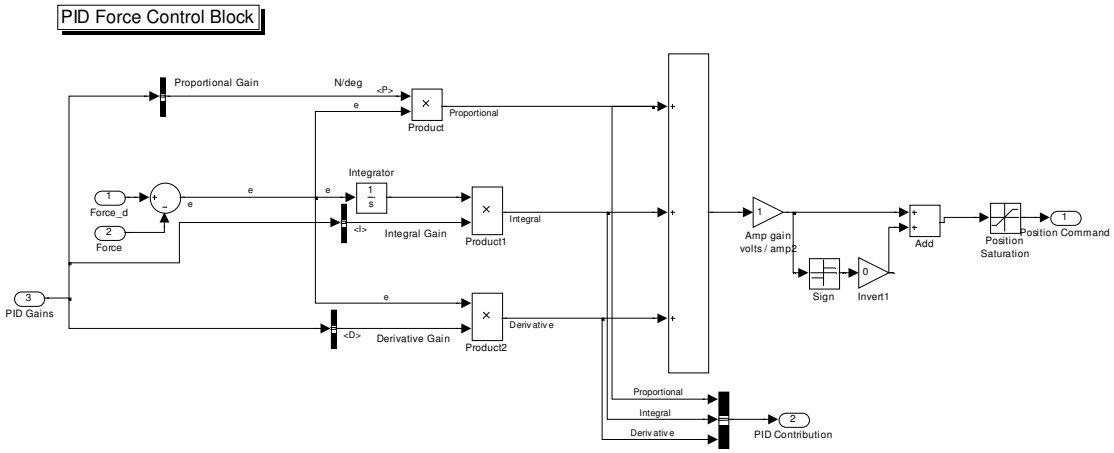

Figure D-4. PID Force Control subblock for torque control diagram for Matlab Simulink.

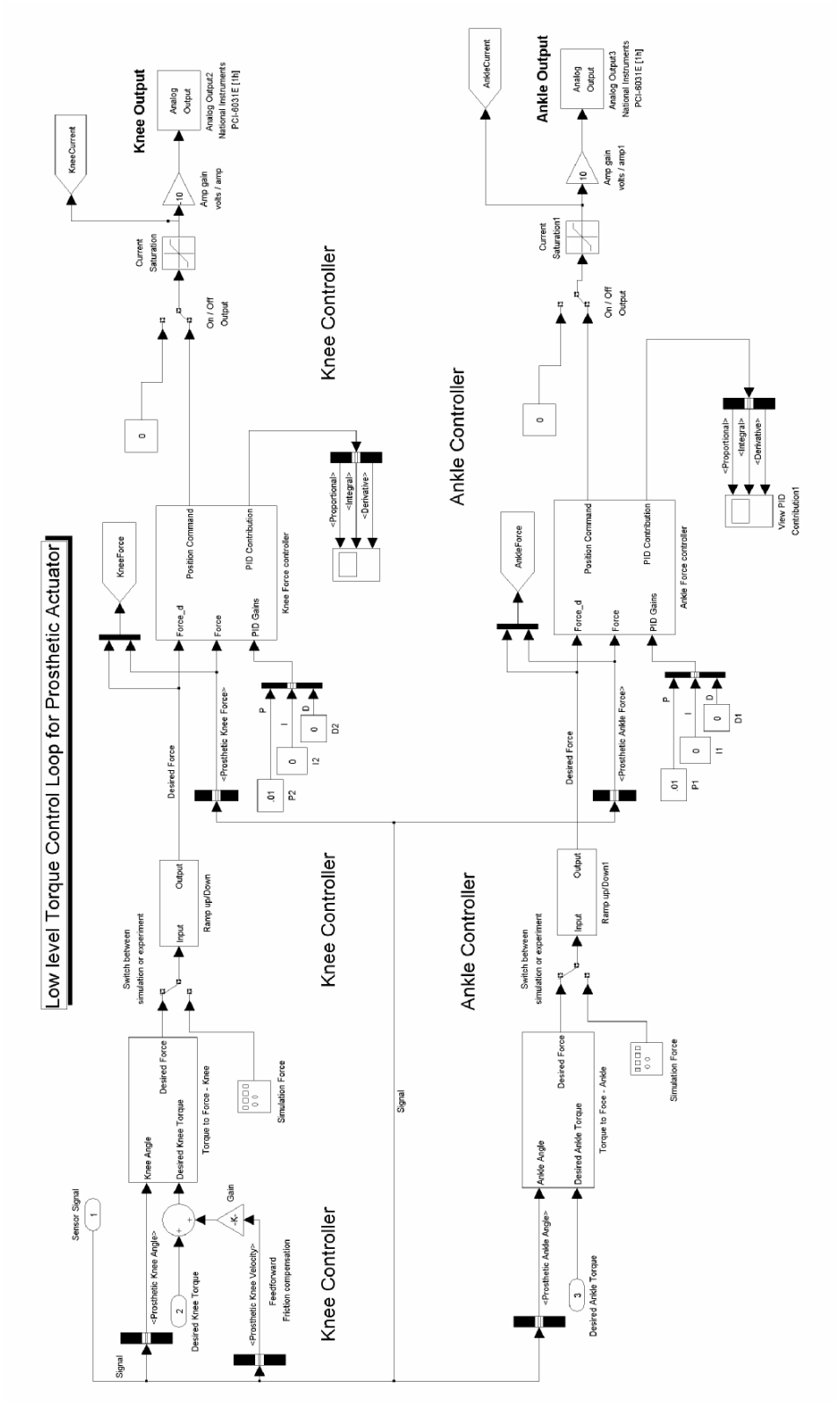

Figure D-5. Torque control diagram for Matlab Simulink.

11. Variable Values

```
%This file contains the constants for Leg Controller variables

%General Simulink Variables
sim_time = 60;     %Length of Simulation
sampling_rate = 1000;
sample_time = 1/sampling_rate;

%%%%%%%%%%%%%%%%%%%%%%%%%%%%%%%%%%%%%%%%%%%%%%%%%%%%%%%%%%%%%%%%%%%%%%%%%%%%

%Signal Conditioning for Prosthetic Leg

%Socket Load Cell Conversion Matrix;
SocketLoadMatrix =
[128.95,-7.0311,1.7243;107.86,28.621,-12.117;64.195,-58.103,25.948;-167.16,50
.542,-18.793;60.458,-14.455,4.3797;-102.93,14.625,-1.6182;-56.624,2.5802,-2.7
663;-49.5,9.5874,-0.67743;-8.3461,6.6598,-0.1948;2.0407,2.2391,-0.31808;-12.7
13,0.3288,6.7424;-17.675,-0.23942,-0.74621;4.7048,-0.34847,1.0689;1.797,0.102
45,0.11055;-0.3911,0.023332,-0.044451;];

%Prosthetics related conversion
prosthetic_ankle_angle_offset = 6.3030; %6.202
prosthetic_knee_angle_offset = 7.810;
zero_axial_load = 0.01;
zero_frontal_moment = 2.524;
zero_sagittal_moment = 2.305;
KneeTorqueZero = -182;
AnkleTorqueZero = -145;

%Force to Torque conversion
%Knee
L1k = .0434;
L2k = 10.875*.0254;
L = 11*.0254;
m = 2.72;
```

```
%Ankle
L1a = 2*.0254;
L2a = 10.875*0.0254;
%%%%%%%%%%%%%%%%%%%%%%%%%%%%%%%%%%%%%%%%%%%%%%%%%%%%%%%%%%%%%%%%%%%%%%%%%%%%

%Gait Detection related variables
%Gyroscope zero voltage
gyro_zero_vel_volt = 2.35;
%Gyro related constants
gyro_pos_threshold = 1; %If gyro pos is greater than 1deg the heel is off

%1. Footswitch threshold
sound_front_threshold = 7;%5;
sound_heel_threshold = 7;
pros_front_threshold = 7;%5;
pros_heel_threshold = 7;

%Axial Load Threshold to distinguish between stance and swing
axial_load_threshold = 1000;
```